A structured procedure for the selection of thermal energy storage options for utilization and conversion of industrial waste heat

Manente, Giovanni; Ding, Yulong; Sciacovelli, Adriano

DOI:
10.1016/j.est.2022.104411

Document Version
Publisher's PDF, also known as Version of record

Citation for published version (Harvard):
Manente, G, Ding, Y & Sciacovelli, A 2022, 'A structured procedure for the selection of thermal energy storage options for utilization and conversion of industrial waste heat', *Journal of Energy Storage*, vol. 51, 104411. https://doi.org/10.1016/j.est.2022.104411

Journal of Energy Storage 51 (2022) 104411

Contents lists available at ScienceDirect

Journal of Energy Storage

journal homepage: www.elsevier.com/locate/est

A structured procedure for the selection of thermal energy storage options for utilization and conversion of industrial waste heat

Giovanni Manente, Yulong Ding, Adriano Sciacovelli *

Birmingham Centre for Energy Storage, School of Chemical Engineering, University of Birmingham, Birmingham, B15 2TT, United Kingdom

ARTICLE INFO

Keywords:
Waste heat recovery
Thermal energy storage
Selection strategy
Power generation
Fluctuating industrial sources
Phase change materials

ABSTRACT

Thermal energy storage is a key enabling technology for the recovery and valorisation of industrial waste heat. Nevertheless, there is a wide gap between the variety of heat storage options investigated and the recurrent few types virtually implemented in the industries. To take advantage of a wider spectrum of solutions, a structured procedure is proposed in this work for the selection of storage material and layout. The algorithm developed consists of a preliminary storage design followed by a performance estimation of the overall system where the heat storage is integrated. The preliminary design allows a first screening and ranking of sensible, latent or thermochemical materials using a quasi-stationary approach. The performance estimation leads to the final selection of the heat storage system, which is based on the analysis of the dynamic thermal response of the heat storage along with physically based or input-output models for the load. The algorithm is applied to improve the heat recovery of a discontinuous and fluctuating flue gas at medium temperature from a steel industry, targeting the production of process steam or electricity. The results show that the integration of a packed bed heat storage, either of the sensible or latent type, allows the highest amount of steam to be generated in the discharging. Moreover, the combination of the same heat storage with an organic Rankine cycle or the Kalina cycle results in the highest amount of generated electricity. The investment in a packed bed rock storage was found to result in payback times of about seven years, whereas tank-based storage units appear not profitable due to the high cost of the silicone oil.

1. Introduction

1.1. Background and state of the art

The recovery and valorisation of the waste heat released to the environment in many industrial processes could displace a significant amount of fossil fuels and accelerate the transition towards carbon neutrality. Nevertheless, the inherent discontinuous and fluctuating patterns of the industrial waste heat sources have widely hindered their utilization and conversion until now. In this context, thermal energy storage (TES) systems can play a key role by decoupling the heat source and the heat utilization/conversion systems. TES applications for industrial waste heat (IWH) recovery were comprehensively reviewed in [1]. Over the past few years, the integration of TES systems in energy intensive industries has been further investigated considering various storage media, as shown in Tables 1 to 6. The table reports the features of the TES system application, with a focus on the operating conditions, heat carriers and operational patter rather than application-specific parameters such as for example, storage efficiency and parasitic losses. The main features of these studies are briefly summarized in the following, focusing on those systems targeting steam production or electricity generation.

Several investigations and real installations of IWH recovery rely on the well-known water tank TES (Table 1), often in combination with low temperature Organic Rankine Cycles (ORCs). Power generation from a discontinuous stream of flushing slag water in blast furnace iron making process was investigated in [2]. A 200 kW ORC was designed in [3] for waste heat recovery (WHR) from the flue gas in a steel processing plant, where the temperature fluctuations were suppressed using a water tank installed in the heat transfer loop of pressurized water. In [4] an indirect TES based on a pressurized water tank was selected for the recovery of intermittent waste heat in a coffee roasting plant. In [5] the WHR from the flue gases of an annealing furnace and galvanization line in a steel industry was assessed. A hot water storage tank was integrated with the purpose of providing a steady thermal power and temperature to the ORC unit. In [6] a dynamic model of a WHR system for steam production from the off-gas of an electric arc furnace (EAF) was developed. A

* Corresponding author.
E-mail addresses: G.Manente@bham.ac.uk (G. Manente), Y.Ding@bham.ac.uk (Y. Ding), A.Sciacovelli@bham.ac.uk (A. Sciacovelli).

https://doi.org/10.1016/j.est.2022.104411
Received 28 September 2021; Received in revised form 9 February 2022; Accepted 10 March 2022
Available online 19 March 2022

Nomenclature

0-D	zero dimensional
1-D	one dimensional
CEPCI	chemical engineering plant cost index
EAF	electric arc furnace
EES	equation engineering solver
HFO	hydrofluoroolefins
HRSG	heat recovery steam generator
HTF	heat transfer fluid
IWH	industrial waste heat
KC	Kalina cycle
LTES	latent thermal energy storage
MADM	multi-attribute decision making
MP	medium pressure
NTU	number of transfer units
ORC	organic Rankine cycle
PCM	phase change material
SAW	simple additive weighting
SE	stirling engine
SM	sensible material
SRC	steam Rankine cycle
STES	sensible thermal energy storage
T	temperature
TCES	thermochemical energy storage
TCM	thermochemical material
TES	thermal energy storage
WHR	waste heat recovery

Symbols

A	(m^2), area
c	(€/kg), specific cost
C	(€), cost
C	(kg/m^3), mass concentration
c_p	(kJ/kg-K), specific heat capacity
D	(m), diameter
E	(kJ), energy
$E_{d,M}$	(kJ/kg), energy density per unit mass
$E_{d,V}$	(kJ/m^3), energy density per unit volume
H	(m), height
K	(/), number of time intervals
L	(m), length
M	(kg), mass
$\dot{m}$	(kg/s), mass flow rate
N	(/), number of time intervals
N	(/), number of nodes/layers
p	(bar), pressure
Per	(m), perimeter
Q	(kJ), quantity of heat
$\dot{Q}$	(kW), rate of heat transfer
t	(s), time
T	(°C), temperature
U	(kW/m^2-K), overall heat transfer coefficient
V	(m^3), volume
$\dot{W}$	(kW), power output
x	(m), Cartesian coordinate

Greek letters

Δt	(s), time step
Δh_{melt}	(kJ/kg), latent heat of fusion
Δh_{react}	(kJ/kg), heat of reaction
ε	(/), effectiveness
ε	(/), void fraction
η	(%), efficiency
λ	(W/m-K), thermal conductivity
ρ	(kg/m^3), density
χ	(/), liquid fraction

Subscripts

amb	ambient
av	available
base	base
ch	charging
cross	cross-sectional
dis	discharging
eff	effective
el	electrical
f	fluid
gas	flue gas
hr	heat recovery
hs	heat source
HTF	heat transfer fluid
HX	heat exchanger
in	inlet
L	layer of phase change material
l	liquid
lat	lateral
load	load
loss	loss
m	material
max	maximum
melt	melting
min	minimum
net	net
out	outlet
ov	overall
pb	packed bed
PCM	phase change material
R	rock layer
react	reaction
s	solid
S	storage
SM	sensible material
TCM	thermochemical material
th	thermal
upg	upgrade
ws	water/steam

thermocline pressurized water storage tank was integrated to ensure a constant supply of steam, despite the batch wise working process of the EAF. While the use of water tanks certainly appears a straightforward heat storage solution, yet it might degrade the temperature level of the waste heat source.

A different TES option, especially used in the steel industry, is the use of steam as storage medium (Table 2). In a real pilot project developed in northern Italy, waste heat was recovered from the off-gas of the EAF to generate medium pressure steam, which was supplied either to a high temperature ORC or the district heating network [7]. A steam accumulator of 150 m^3 volume was included to smooth the fluctuations in steam supply. A similar plant was built in Germany as reported in [8]. However, the large volumes required raise concerns about the viability of the steam storage in other industries.

For WHR at medium to high temperatures, liquid or solid sensible storage media are available. While the use of thermal oil up to

Table 1
Applications of the water tank for industrial WHR.

Application	Heat source/s	Pattern	Mass flow rate heat source (kg/s)	Temperature heat source (°C)	Heat carrier charging	Type of storage	Storage material/ fluid	Storage volume (m^3)	Heat carrier discharging	Heat sink	Selected/ optimal working fluids	Power output (kW_e)	Reference
Steel industry – blast furnace	Flushing slag water	Discontinuous	656.3	85	Flushing slag water	Tank indirect (uniform temperature)	Pressurized water	/	Working fluid ORC	Low T ORC	Butane, R245fa, R141b	3300	[2]
Steel processing plant – painted steel sheets	Flue gas (from a regenerative thermal oxidizer)	Fluctuating temperature and flow rate	4.9–14.2	177–265	Pressurized water	Tank direct (perfectly mixed, constant mass)	Pressurized water	1	Pressurized water	Low T ORC	R245fa	200	[3]
Steel industry – heating of steel plates	Flue gases (from annealing furnace and galvanization line)	Fluctuating temperature and flow rate	9.2 (design)	160–440	Pressurized water	Tank direct (perfectly mixed, variable mass)	Pressurized water	100	Pressurized water	Low T ORC	Opteon 1100 (HFO)	~150	[5]
Food industry – coffee roasting	Flue gas	Fluctuating flow rate	0.8–1.5	350–400	Flue gas	Tank indirect (uniform temperature)	Pressurized water	0.5	Pressurized water	Low T ORC	Butane, pentane, R227ea, R245fa, R1234ze	25–30	[4]
Steel industry – scrap melting	Off-gas (from the electric arc furnace)	Fluctuating temperature and flow rate	/	max 1200 °C	Pressurized water (200 °C)	Tank direct (stratified)	Pressurized water	/	Pressurized water	Saturated steam at 7 bar (a) fed into a steam network	/	/	[6]

Table 2
Applications of the steam tank for industrial WHR.

Application	Heat source/s	Pattern	Mass flow rate heat source (kg/s)	Temperature heat source (°C)	Heat carrier charging	Type of storage	Storage material/fluid	Storage volume (m^3)	Heat carrier discharging	Heat sink	Selected/optimal working fluids	Power output (kW_e)	Reference
Steel industry – scrap melting	Off-gas (from the electric arc furnace)	Discontinuous and fluctuating	16.6 (avg.)	505 (avg.)	Water/steam (17–25 bar (a))	Steam tank	Steam (11–25 bar (a))	150	Steam/water	District heating network/High T ORC	Hexamethyl-disiloxane	1800	[7]
Steel industry – scrap melting	Off-gas (from the electric arc furnace)	Discontinuous and fluctuating	/	Max 1600 °C	Water/steam (27 bar(a))	Steam tank	Steam	/	Steam/water	Steam for adjacent industry/high T ORC	N.A.	2700	[8]

Table 3
Applications of the thermal oil tank or molten salt tank for industrial WHR.

Application	Heat source/s	Pattern	Mass flow rate heat source (kg/s)	Temperature heat source (°C)	Heat carrier charging	Type of storage	Storage material/fluid	Storage volume (m^3)	Heat carrier discharging	Technology	Selected/optimal working fluids	Power output (kW_e)	Reference
Steel industry – scrap melting	Off-gas (from the electric arc furnace)	Fluctuating temperature and flow rate	/	max 1200 °C	Molten salt	Two-tank direct (variable mass)	Molten salt	/	Molten salt	SRC	Steam	5000	[9,10]
Cement industry	Hot air (from clinker cooling)	Fluctuating temperature	53.9	180–330	Therminol VP-1	Single tank direct (perfectly mixed, constant mass)/Two-tank direct (variable mass)	Therminol VP-1	170–1100	Therminol VP-1	Low T ORC	Pentane	N.A.	[24]
Steel industry – scrap melting	Off-gas (from the electric arc furnace)	Fluctuating temperature and flow rate	14–22	110–730	Molten salt (HITEC)	Two-tank direct (variable mass)	Molten salt (HITEC)	7	Molten salt (HITEC)	High T ORC	Toluene	N.A.	[24]
Steel industry – billet reheating	Flue gas (from a billet reheat furnace)	Fluctuating flow rate	3.3–8.7	400 (avg.)	Therminol VP-1	Two-tank direct (variable mass)	Therminol VP-1	20	Therminol VP-1	High T ORC	Toluene	~500	[24,25]

Table 4
Applications of the solid media for industrial WHR.

Application	Heat source/s	Pattern	Mass flow rate heat source (kg/s)	Temperature heat source (°C)	Heat carrier charging	Type of storage	Storage material/ fluid	Storage volume (m^3)	Heat carrier discharging	Technology	Selected/ optimal working fluids	Power output (kW_e)	Reference
Industrial waste heat	N.A.	Fluctuating	0.8	600	Hot air	Packed bed	Sand	3	Ambient air	High T ORC	Toluene	78–94	[14]
Industrial waste heat recovery	Flue gas	Constant (during the experimental campaign)	0.58	525	Air	Packed bed (horizontal)	Refractory ceramic (bauxite rubbles)	9	Air	Any (discharge temperatures up to 525 °C)	/	/	[12]
Steel industry – scrap melting	Off-gas (from the electric gas furnace)	Fluctuating temperature and flow rate	0.94–2.88	700	Air	Packed bed	Steel slag	3	Air	Any (discharge temperatures up to 700 °C)	/	/	[13]
Aluminium industry	Flue gas from aluminium furnaces	Fluctuating temperature and flow rate	0.4–3.8	650–800	Flue gas	Solid block	1)Cast iron 2)Concrete	6.4	Thermal oil (Dowtherm A)	Low T ORC	R245fa Isopentane	86–323	[11]

350–400 °C is quite established, the use of molten salts or liquid metals for heat storage at higher temperatures is less proven in industrial contexts (Table 3). Indeed, one of the few investigations about the use of molten salt as heat transfer and storage material in the industry was reported in [9,10], addressing WHR from the EAF. The system included an off-gas to salt heat exchanger, hot and cold molten salt tanks, a molten salt steam generator and a 5 MW steam turbine. With regards to solid materials, concrete, ceramic or sand are highly investigated since they potentially represent cheaper storage options (Table 4). In [11] a concrete block was selected for WHR from the fluctuating flue gas of aluminium furnaces. A large scale air-ceramic packed bed for storage of high temperature industrial waste heat up to 600 °C was designed and tested in [12], which reached a 90% heat recovery. In [13] a TES system based on a packed bed using steel slag as storage material was proposed to achieve a continuous heat supply from the batch operation of a steel furnace. In [14] a packed bed TES made of sand particles was combined with a high temperature ORC.

Alternatively, the use of Phase Change Materials (PCMs) at medium to high temperatures (molten salts or metals) increasingly appear ready to expand their outreach from lab/prototype sizes to real scale storage systems (Table 5). For example, a thermal flywheel system was proposed in [15], which exploited the characteristics of a metal PCM (aluminium) to reduce the variability of the off-gas temperature in EAF steel plants, and, ultimately, improve the heat-to-power efficiency using a steam Rankine cycle (SRC). In [16] the impact of retrofitting a similar PCM-based technology to improve the WHR using an ORC in a steel billet reheating furnace was investigated. A very high temperature application of PCMs was devised in [17] to improve the recovery from the hot flue gases in the ceramic industry.

More sophisticated thermal energy storage options rely on the use of thermochemical reactions (Table 6). The integration of an adsorption TES based on zeolite 13× into a batch brewery process was investigated in [18]. At higher temperatures, a thermochemical energy storage (TCES) based on magnesium hydroxide ($Mg(OH)_2$) within a combined cycle power plant supplying heat and power to a paper mill was investigated in [19]. Due to the heat storage, the plant could switch from a heat-controlled to a power-controlled mode, taking advantage of the changing electricity spot prices. In [20] a TCES based on calcium hydroxide ($Ca(OH)_2$) was proposed for off-gas WHR in EAF steelmaking to achieve a high heat storage density and a high heat extraction temperature for efficient power generation in a SRC. These certainly represent promising systems, however they require a deeper level of integration in the overall industrial process to reach a high storage efficiency.

1.2. Motivation of this work

It clearly appears from the literature review that multiple heat storage options are potentially available for any given industrial waste heat source, while targeting the supply of process steam or the generation of electricity. However, in spite of the relatively high number of specific case studies, only a few papers propose systematic methods for the selection of TES systems in industrial settings, which are briefly discussed here. The general procedure presented in [21] relied on a preliminary selection of the storage materials, based on their properties and the storage purpose (e.g. long term or short term storage), followed by a ranking based on one or more objective functions related to the storage itself (e.g. energy stored per unit volume and cost). In [22] the selection of PCMs for latent heat storage was based on three consecutive steps, namely pre-screening using qualitative properties, ranking using quantitative properties and performance objective examination. The latter was carried out using the energy density, the heat stored per unit cost and the thermal diffusivity as objective functions. It clearly emerges that both these methodologies focus on performance objectives which are strictly related to the storage itself, while they overlook those relevant to the wider system where the storage is integrated. In this regard, the theoretical method to identify the optimal melting temperature of

Table 5
Applications of medium-high temperature PCMs for industrial WHR.

Application	Heat source/s	Pattern	Mass flow rate heat source (kg/s)	Temperature heat source (°C)	Heat carrier charging	Type of storage	Phase change material (PCM)	Storage volume (m^3)	Heat carrier discharging	Technology	Selected/ optimal working fluids	Power output (kW_e)	Reference
Cement industry	Hot air (from clinker cooling)	Fluctuating temperature	53.9	180–330	Hot air	N.A. (cylindrical tubes filled with PCM)	$LiNO_3$ (T_{melt} = 254 °C)	31	Hot air	High T ORC	Hexamethyl-disiloxane	N.A.	[24]
Steel industry – scrap melting	Off-gas (from the electric arc furnace)	Fluctuating temperature and flow rate	14–22	110–730	Off-gas	N.A. (cylindrical tubes filled with PCM)	50%NaCl-50%$MgCl_2$ (T_{melt} = 450 °C)	4.5	Off-gas	High T ORC	Toluene	N.A.	[24]
Steel industry – scrap melting	Off-gas (from the electric gas furnace)	Fluctuating temperature	60.2	220–950 600 (avg.)	Off-gas	Cylindrical pipes filled with PCM	Aluminium (T_{melt} = 660 °C)	8.5	Off-gas	SRC (40 bar/400 °C)	Steam	6000	[15]
Steel industry – scrap melting	Off-gas (from the electric gas furnace)	Fluctuating temperature	46.9	390–990 690 (avg.)	Off-gas	PCM in the gap between two coaxial pipes	Al-12%Si (T_{melt} = 576 °C)	20	Off-gas and CO_2	SRC (40 bar/400 °C)	Steam	8640	[26]
Steel industry – billet reheating	Flue gas	Fluctuating flow rate	1.8–8.1	850	Flue gas	PCM in the gap between two coaxial pipes	Al-12%Si (T_{melt} = 576 °C)	1	Recirculated flue gas	High T ORC	Hexamethyl-disiloxane	555	[16]
Ceramic industry – smelting furnace	Flue gas	N.A.	0.26	1100	Flue gas	PCM in the gap between two coaxial tubes	PCM (T_{melt}= 885 °C)	2.5	Combustion air	Combustion air heating up to 865 °C	/	/	[17]

Table 6
Applications of thermochemical materials for industrial WHR.

Application	Heat source/s	Pattern	Mass flow rate heat source (kg/s)	Temperature heat source (°C)	Heat carrier charging	Type of storage	Storage material/fluid	Storage volume (m^3)	Heat carrier discharging	Technology	Selected/optimal working fluids	Power output (kW_e)	Reference
Steel industry – scrap melting	Off-gas (from the electric gas furnace)	Fluctuating temperature and flow rate	25.7–37.8	250–1400	Off-gas	Entrained flow and fluidized bed reactors	TCM Calcium hydroxide ($Ca(OH)_2$)	6.5	Steam	SRC (70 bar/450 °C)	Steam	2800	[20]
Cogeneration unit (biogas engine) in breweries	Exhaust gas	Continuous	/	250	Thermal oil	Closed system	TCM (Zeolite 13×)	/	Thermal oil	Process heat at 120 °C	/	/	[18]
Combined cycle power plant	Live steam HRSG	Discontinuous	/	510	Live steam HRSG	Fluidized bed reactor	TCM ($Mg(OH)_2$)	/	Water/steam	Process heat at 160 °C paper mill	/	/	[27]

PCMs in WHR applications recently developed in [23] extend the analysis to the heat source and the heat engine. However, there is no mention in that work to the type of the storage material nor to the storage configuration. Also, the use of the Curzon-Ahlborn efficiency to assess the efficiency of the heat engine appears questionable since any difference in performance of different power cycles is suppressed. A more pragmatic approach was used in [24] to compare sensible and latent TES systems for industrial WHR and power generation using the ORC heat engine. In spite of the limited number of storage configurations and the use of a predefined set of storage materials, the authors could demonstrate the economic and environmental advantages deriving from a suitable storage selection.

In general, there is a lack of organized procedures for the selection of TES systems in WHR applications, which take into account the mutual interaction between heat source and heat storage as well as the mutual interaction between heat storage and heat utilization system. This has the wider implication that the intermittent and fluctuating heat sources, typical of the industrial processes, are either wasted or combined with well-established heat storage technologies (e.g. water tank), without exploring the potential advantages deriving from the variety of available storage materials and configurations. Moreover, the heat utilization/conversion technology is generally fixed a priori, without considering the impact that the particular selection of the heat storage can have on its viability and performance.

1.3. Contribution and novelty of this work

This work addresses these shortcomings by proposing a systematic method for the effective recovery of discontinuous and/or fluctuating industrial waste heat sources through the proper selection of the material and configuration of the heat storage. The method is based on an algorithm composed of a sequence of ten operations, which progressively lead to the selection of the most suitable storage option to meet the demand of process heat or electrical power. The screening and ranking of the storage materials are performed in a first phase using a quasi-stationary approach, which assesses the capability of extracting heat from the waste heat source in addition to the material properties, and generates a preliminary storage design for the best material candidates. The performance objective assessment is performed at system level, rather than at storage level, in a second phase by considering the dynamic thermal response of the heat storage in the charging and discharging processes as well as the performance of the heat utilization system. This is done using well established zero dimensional (0-D) or one dimensional (1-D) models of the heat storage and taking advantage of simulation/performance models specifically developed for different heat utilization/conversion systems. For this purpose, the optimum trends of thermal efficiency and heat recovery effectiveness of several heat to power technologies have been obtained in a wide temperature range. By extending the investigation boundaries to the heat source and the heat utilization system, the benefits deriving from the integration of the heat storage can be simply assessed by an energetic analysis that compares the system outputs (steam, electricity) to the waste heat available. On the other hand, the storage design features (e.g. volume, cost), which are available from the preliminary design and are adjusted based on the results of the performance estimation, are taken into account in the search of the maximum performance or economic benefit associated with the storage integration.

Besides improving the design of the waste heat recovery process at an early conceptual stage, the proposed algorithm lays the foundation for a general software tool that automatizes the storage selection and integration in industrial environments. In this work the algorithm is applied considering a limited, yet already meaningful, set of sensible and latent heat storage materials and layouts for utilization of medium temperature flue gases from a steel processing plant. It is shown how the structured procedure leads to the choice of the most suitable storage option for the production of process steam, or the best combination heat

storage - heat engine when targeting the production of electricity.

2. Methodology

2.1. General description of the structured procedure

An original structured procedure is developed in this work for the selection among thermal energy storage options in WHR applications, which consists of a preliminary storage design followed by the evaluation of the performance at system level. A general flowchart of the overall procedure is shown in Fig. 1.

2.1.1. Preliminary design of the heat storage

The preliminary design of the heat storage unit is performed using a quasi-stationary approach and a limited set of input parameters. It can be easily managed using an Excel spreadsheet. According to the flowchart in Fig. 2, it involves the screening and ranking of the storage materials based on: i) the parameters of the heat source; ii) the type of heat load; iii) the material properties. The selection of the storage layout is performed as the seventh step, which is shown in a separate flowchart in Fig. 3.

The meaning and the calculations involved in each step of the algorithm are described in the following.

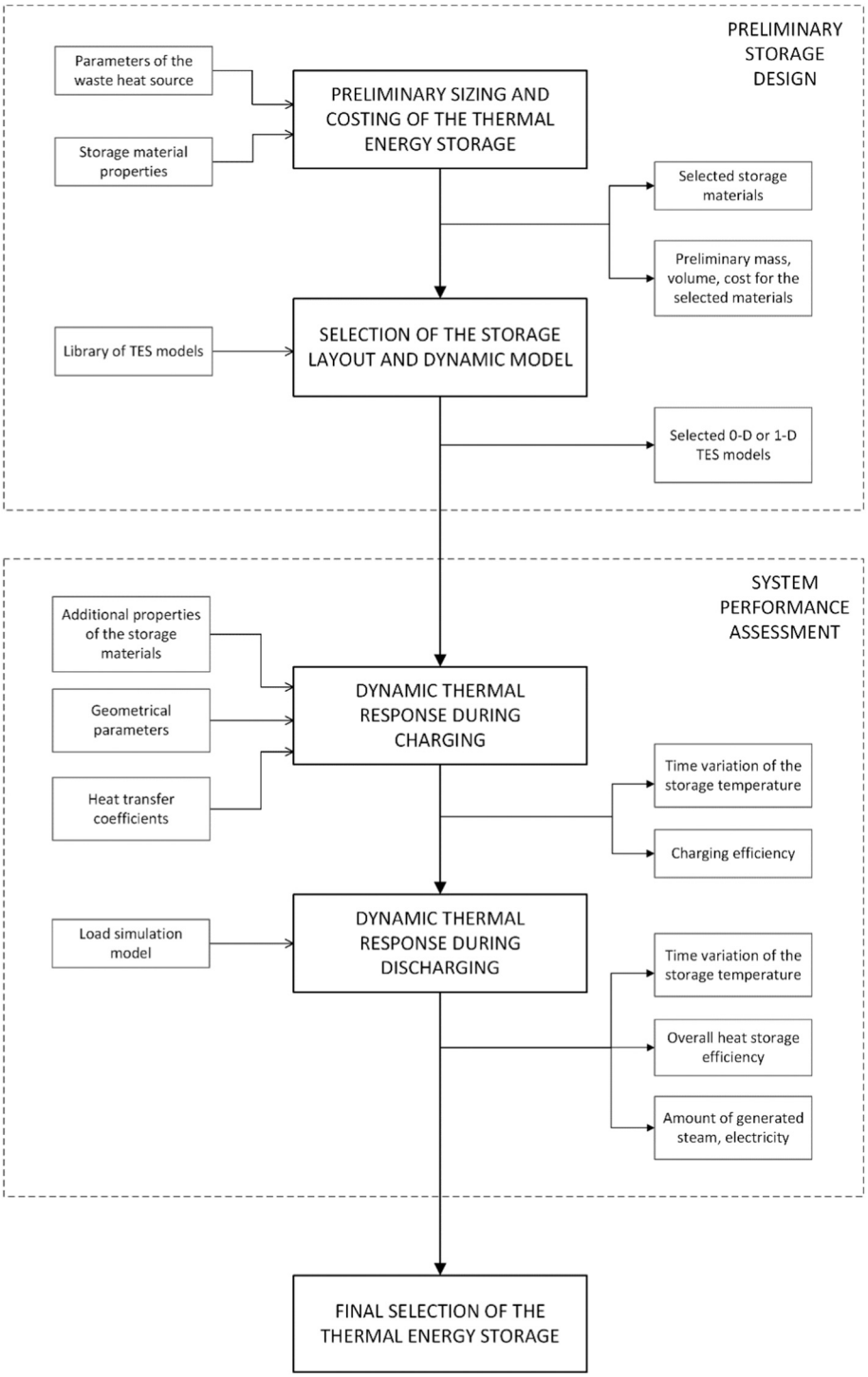

Fig. 1. Flowchart of the proposed procedure for heat storage selection.

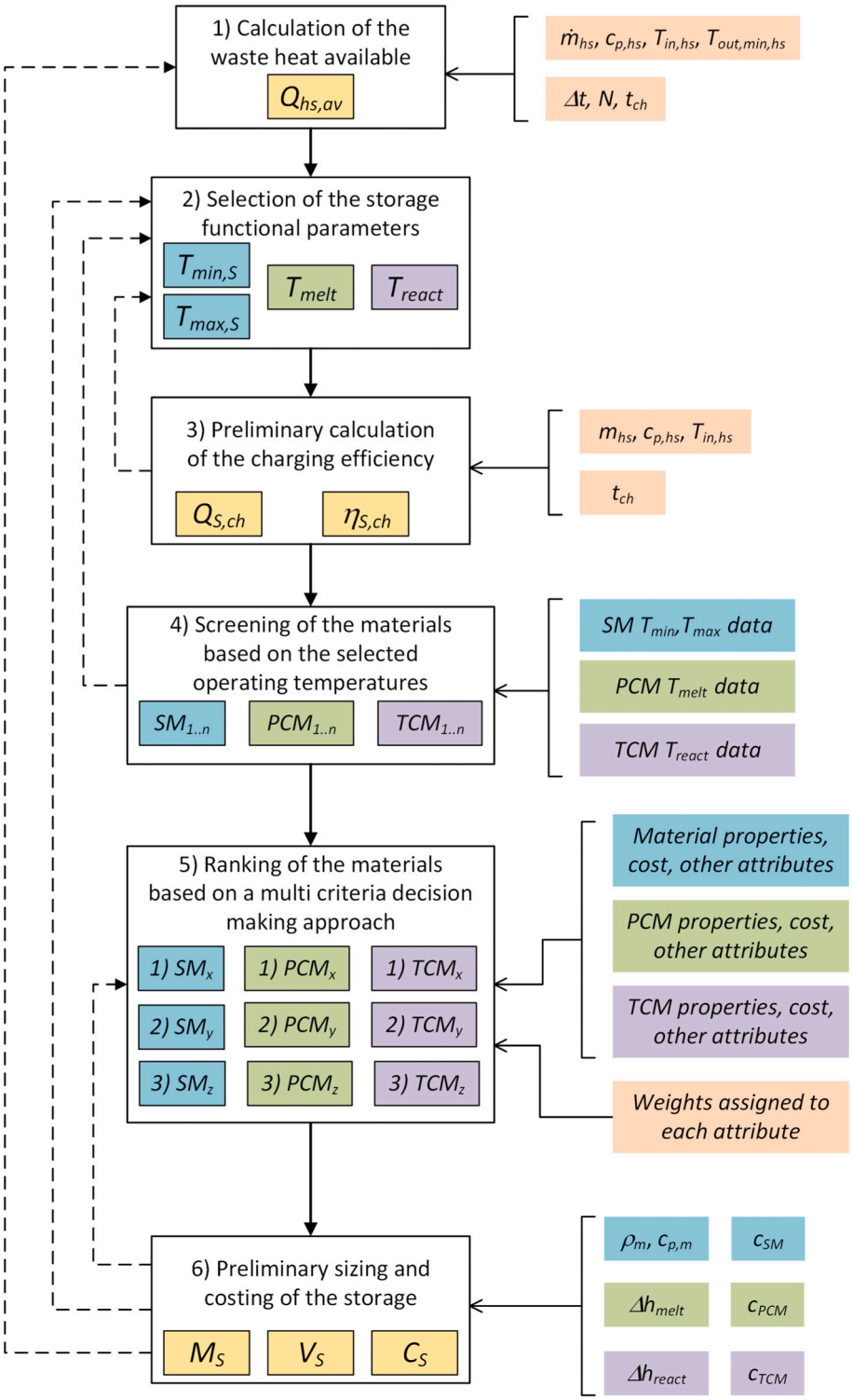

Fig. 2. Flowchart of the proposed algorithm for the preliminary storage design. The box colours refer to sensible storage (light blue), latent heat storage (green), thermochemical storage (violet). The general input and output parameters are enclosed within pink and yellow boxes, respectively. (For interpretation of the references to colour in this figure legend, the reader is referred to the web version of this article.)

I. The first step is the calculation of the thermal energy available from the industrial waste heat. Due to the fluctuating pattern of most industrial waste heat sources, the time domain is subdivided in N time intervals, where the inlet temperature and mass flow rate can be considered constant. On the other hand, the extent of utilization of IWH sources is usually constrained by a minimum temperature, due to the further processing downstream or to prevent the occurrence of undesired effects. Since the time duration (e.g. a few hours) in which the IWH is available is generally known from the processing time of manufacturing processes, this time can be used as the charging time for the preliminary sizing of the storage system. Thus, the waste heat available to the thermal energy storage is:

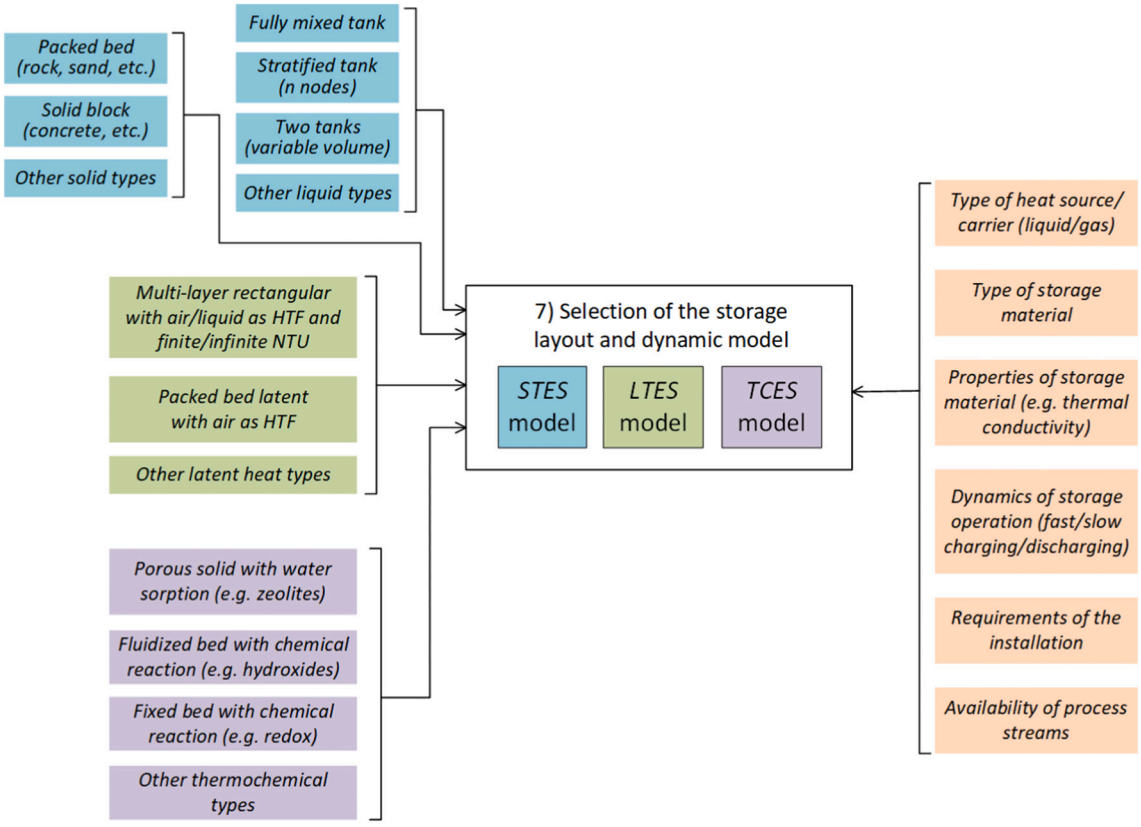

Fig. 3. Flowchart of the seventh step of the algorithm: selection of storage layout and simulation model. For the meaning of the box colours the reader is referred to the legend of Fig. 2.

$$Q_{hs,av} = \sum_{N} \dot{m}_{hs} \cdot c_{p,hs} \cdot \left(T_{in} - T_{out,min}\right)_{hs} \cdot \Delta t \tag{1}$$

where the selected charging time is:

$$t_{ch} = N \cdot \Delta t \tag{2}$$

II. The second step is the selection of the functional parameters of the heat storage, which are temperatures or temperature intervals. This selection is driven by the need of recovering the highest amount of the waste heat available, while not degrading its quality (i.e., exergy) to meet the load requirements. The functional parameters of sensible TES are the minimum and maximum storage temperatures. The former ($T_{min,S}$) is selected as the minimum temperature to enable load operation, the latter ($T_{max,S}$) is set high, consistently with the heat source inlet temperature, to minimize the amount and cost of storage material. The functional parameter of latent TES is the melting temperature (T_{melt}), which must be higher than the temperature required by the load, yet fairly low for an effective heat extraction from the waste heat source. The functional parameter of TCES is the reaction temperature (T_{react}) of the thermochemical material, which must fulfil similar requirements. Note that the availability of storage materials matching these temperatures is not considered at this stage to avoid any bias in the selection of the functional parameters.

III. The third step is the preliminary calculation of the charging efficiency. A first estimate of the heat transferred from the waste heat source to the thermal energy storage in the charging process ($Q_{S,ch}$) can be obtained using the following equations:

$$\begin{cases} Q_{S,ch} = \sum_{N} \dot{m}_{hs} \cdot c_{p,hs} \cdot \left(T_{in,hs} - T_{min,S}\right) \cdot \Delta t & sensible \\ Q_{S,ch} = \sum_{N} \dot{m}_{hs} \cdot c_{p,hs} \cdot \left(T_{in,hs} - T_{melt}\right) \cdot \Delta t & latent \\ Q_{S,ch} = \sum_{N} \dot{m}_{hs} \cdot c_{p,hs} \cdot \left(T_{in,hs} - T_{react}\right) \cdot \Delta t & thermochemical \end{cases} \tag{3}$$

which clearly show how the maximum extent of waste heat recovery is limited by the selection of the functional parameters. Accordingly, a preliminary evaluation of the charging efficiency can be obtained:

$$\eta_{S,ch} = \frac{Q_{S,ch}}{Q_{hs,av}} \tag{4}$$

The selection of the functional parameters can be revised based on the obtained value of charging efficiency (see the dashed arrowed line in the flowchart of Fig. 2).

IV. The fourth step consists in a first screening of the storage materials based on the selected functional parameters. The operational temperature limits of solid and liquid storage media, the melting temperatures of phase change materials (PCMs) and the reaction temperatures of thermochemical materials (TCMs) are provided to the algorithm by a database of storage material properties in-house developed from a literature survey (see the supplementary material), which covers both low and medium/high temperature applications. By cross-checking these data against the selected functional parameters, a shortlist of sensible, latent and thermochemical materials can be obtained. Based on the availability of a suitable number of storage materials, the decisions taken at step 2 can be further revised.

V. The fifth step is the ranking of the screened storage materials based on their properties (thermophysical, chemical, etc.),

specific cost, as well as other attributes related to the environmental impact, safety, etc., which are provided by the database. A multi-attribute decision making method (see Appendix A) is applied to systematically rank the materials, where a weight is given to each attribute that determines the importance of each attribute relatively to each other. The performance ranking of materials is obtained by considering the score reached by each of them.

VI. The sixth step is the preliminary sizing and costing of the storage for the selected set of materials. The preliminary storage mass (M_S) is obtained from the first estimate of charging heat (Eq. (3)), as follows:

$$\begin{cases} M_S = \dfrac{Q_{S,ch}}{c_{p,m}\cdot(T_{max}-T_{min})_S} & sensible \\ M_S = \dfrac{Q_{S,ch}}{\Delta H_{melt}} & latent \\ M_S = \dfrac{Q_{S,ch}}{\Delta H_{react}} & thermochemical \end{cases} \quad (5)$$

The storage volume (V_S) is the ratio between storage mass and mass density of the storage material:

$$V_S = \frac{M_S}{\rho_{SM/PCM/TCM}} \quad (6)$$

The storage material cost (C_S) is the product of the specific cost per unit weight of the storage material and the storage mass:

$$C_S = c_{SM/PCM/TCM}\cdot M_S \quad (7)$$

If the calculated values of storage mass, volume or cost are deemed too high and not acceptable, one or more of the assumptions and decisions taken at the previous steps are revised, starting from the charging time (see the dashed arrowed lines in Fig. 2). Note that the preliminary storage mass and volume calculated at this step are only used as initial values in the system performance assessment part of the procedure.

VII. The seventh step is about the selection of the thermal energy storage layout/configuration and the related simulation model among a predefined library (Fig. 3). The layout plays a key role in the thermal performance of the storage unit as well as in the performance of the overall system where the storage is integrated. On the other hand, the simulation models provide a more or less accurate approximation of the real behaviour of the storage units and enable the evaluation of their transient thermal response. The selection is based on the type of heat source/carrier (liquid or gas); type and properties of the storage material; dynamics of storage operation (fast or slow charging/discharging); type of installation; availability of process streams (e.g. steam, humidified air, etc.). On the basis of these inputs, the algorithm orientates towards one or more zero-dimensional (0-D) or one-dimensional (1-D) storage models, which have been considered adequate in this work for the performance analysis at system level.

2.1.2. Performance evaluation of the overall heat recovery system

The performance evaluation is based on a sequence of three additional steps that follow the preliminary design, as described below.

VIII. The eighth step is the evaluation of the transient response of the storage unit in the charging process, which is obtained by running the selected simulation model/s. The additional input data required are quite limited due to the simplified (0-D, 1-D) storage models considered. As can be seen from Fig. 4, they are related to: a) time step and number of spatial nodes for the numerical

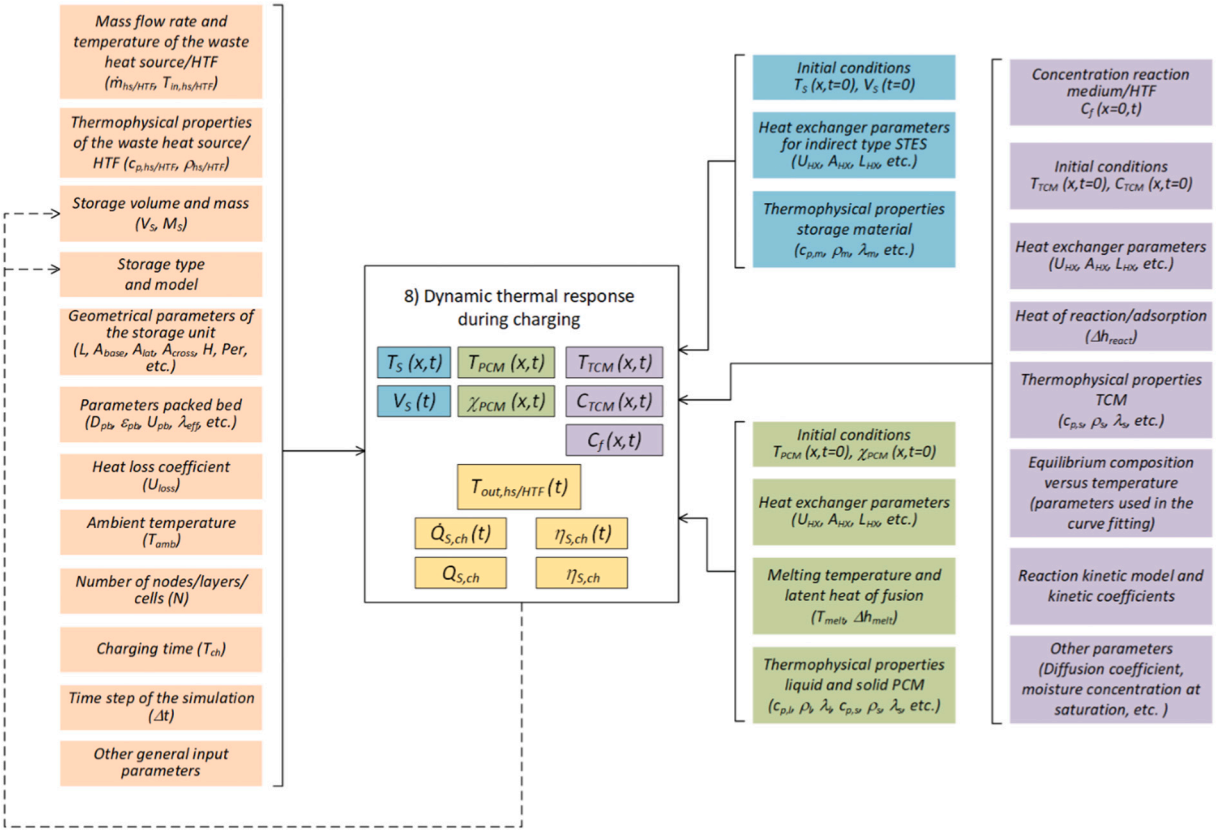

Fig. 4. Flowchart of the eighth step of the algorithm: evaluation of the transient thermal response during the charging process. For the meaning of the box colours the reader is referred to the legend of Fig. 2.

solution; b) thermophysical/chemical properties of the storage material; c) geometrical parameters to evaluate the surface area of heat loss, the surface area of the heat exchangers (for indirect type storage), and the passage area; d) the heat transfer coefficients; e) the kinetic model and other parameters for TCES.

The outputs of the storage simulation models in this step are:

- Time and spatial variation of: storage temperature (sensible, latent and thermochemical), PCM solid/liquid fraction (latent heat storage); concentration of the reactive species (thermochemical);
- Time variation of the storage volume (sensible only with variable volume);
- Time variation of the temperature of the heat source/carrier exiting the storage;
- Time variation of the heat transfer rate from the heat source/carrier to the storage material:

$$\dot{Q}_{S,ch}(t) = \dot{m}_{HTF} \cdot c_{p,HTF} \cdot (T_{in} - T_{out})_{HTF} \tag{8}$$

- Instantaneous charging efficiency:

$$\eta_{S,ch}(t) = \frac{\dot{Q}_{S,ch}}{\dot{Q}_{hs,av}} \tag{9}$$

- Thermal energy transferred from the heat source/carrier to the storage media during the charging time:

$$Q_{S,ch} = \sum_{N} \dot{Q}_{S,ch} \cdot \Delta t \tag{10}$$

- Charging efficiency:

$$\eta_{S,ch} = \frac{Q_{S,ch}}{Q_{hs,av}} \tag{11}$$

The obtained values of: i) storage temperature at the end of the charging process (i.e. the maximum temperature), ii) heat transferred from the heat source/carrier to the storage, and iii) charging efficiency can be compared with the initial estimates of the preliminary design. The storage mass/volume as well as the selection of the layout can be adjusted/revised to improve the transient response (see the two dashed arrowed lines in Fig. 4).

IX. The ninth step assesses the transient thermal response in the discharging using the storage simulation model/s along with a load simulation model. The latter can be either physically based or an input-output model based on transfer functions. The flowchart in Fig. 5 highlights the additional inputs required for this step. In particular, the mass flow rate of the heat transfer fluid can be controlled to match the load demand. Moreover, the end of the discharging process is determined by the threshold temperature, which is the minimum temperature of the heat carrier at storage outlet that enables a proper operation of the load. Since in most of the applications the heat carrier operates in a closed loop on the load side, a simultaneous solution of the storage model and the load model is required, where the outlet temperature from the load is used as input in the storage model.

The main outputs of the ninth step of the algorithm are:

- Time and spatial variation of the storage temperature (sensible, latent and thermochemical), PCM solid/liquid fraction (latent heat storage); concentration of the reactive species (thermochemical).
- Time variation of the storage volume (only variable volume sensible).

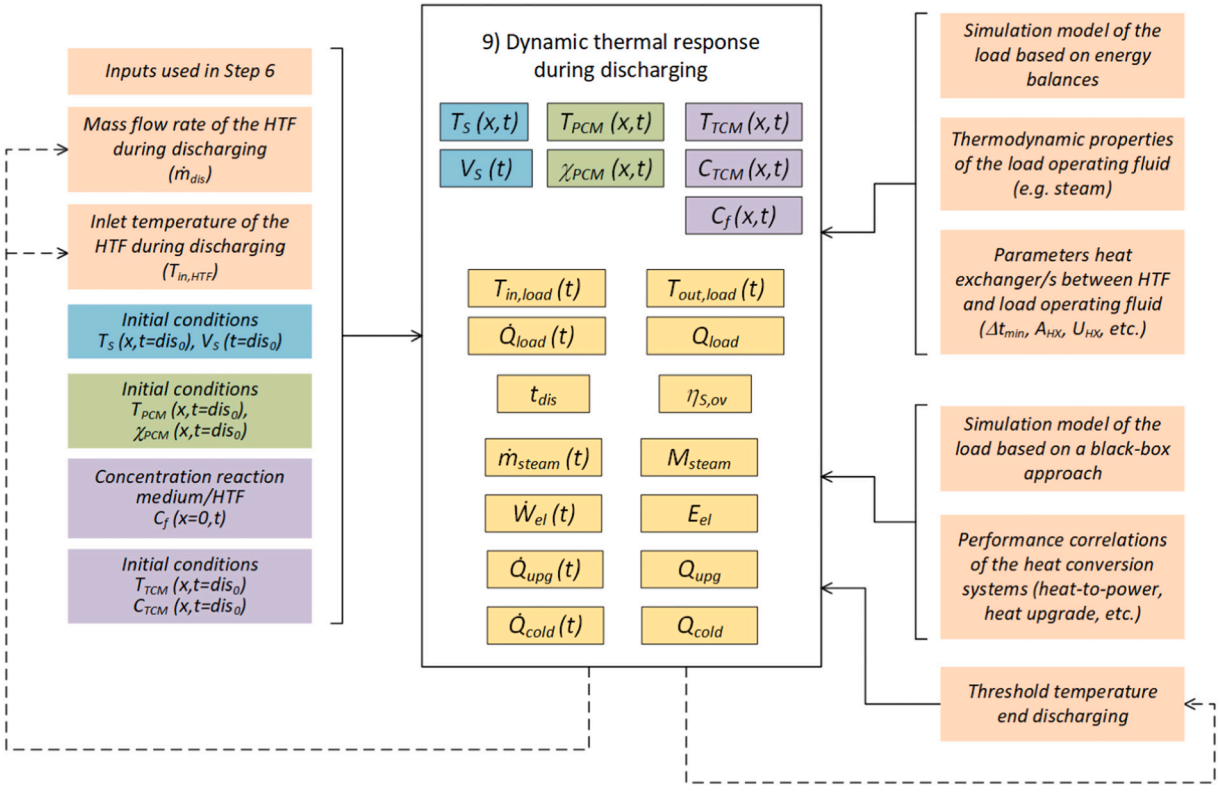

Fig. 5. Flowchart of the ninth step of the algorithm: evaluation of the transient thermal response during the discharging process. For the meaning of the box colours the reader is referred to the legend of Fig. 2.

- Time variation of the temperature of the HTF exiting the storage and entering the load.
- Time variation of the temperature of the HTF exiting the load and recirculated to the storage.
- Time variation of the heat transfer rate from the heat carrier to the load:

$$\dot{Q}_{load}(t) = \dot{m}_{dis} \cdot c_{p,HTF} \cdot (T_{in} - T_{out})_{load} \quad (12)$$

- Thermal energy transferred to the load:

$$Q_{load} = \sum_{K} \dot{Q}_{load} \cdot \Delta t \quad (13)$$

where the discharging time is:

$$t_{dis} = K \cdot \Delta t \quad (14)$$

- Overall heat storage efficiency, which is the ratio between heat transferred to the load and heat available from the heat source:

$$\eta_{S,ov} = \frac{Q_{load}}{Q_{hs,av}} \quad (15)$$

Furthermore, the simulation model of the load provides other performance parameters that are used to assess the performance of the overall heat recovery system where the storage is integrated. For example, if the discharging heat is used to generate medium pressure steam, then it is possible to evaluate the time variation of the steam mass flow rate during the discharging process as well as the total amount of raised steam. Similarly, for heat-to-power generation systems the time variation of the power output and the electricity generated can be calculated using the following equations:

$$\dot{W}_{el}(t) = \dot{Q}_{load} \cdot \eta_{th} \quad (16)$$

$$E_{el} = \sum_{K} \dot{W}_{el} \cdot \Delta t \quad (17)$$

where η_{th} is the thermal efficiency of the heat-to-power system. Similar considerations may be applied to heat upgrade systems and thermally driven refrigeration systems by using appropriate values of the coefficient of performance.

X. The tenth step of the algorithm is the final selection of the most suitable storage unit, which is based on the performance of the overall heat recovery system as well as on the features of the storage itself. In the absence of particular constraints related to the cost or size, the choice may fall on the storage unit which allow the maximum production of steam or electricity. More likely, an economic analysis is carried out to calculate the financial indicators associated with the installation of the heat storage.

2.2. Application of the methodology to a case study

The proposed methodology is applied in this work to the recovery of the waste heat from the flue gas of the steel billet reheating furnace reported in [16]. In the present work the focus is on the flue gas downstream of the air preheater, whose trends of mass flow rate and temperature are shown in Fig. 6. The flowrate is highly variable whereas the fluctuations of the flue gas temperature, around 400 °C, are milder. The manufacturing process runs 15 h per day with a two-shift schedule and it is suspended during nighttime.

In the considered case study, the waste heat generated by the steel industry during the day is stored and later used in the nighttime to provide process steam at 7 bar(a) and 180 °C (first scenario) or electricity (second scenario) to a continuous process of a nearby chemical industry, which heavily relies on fossil fuels (natural gas and diesel) for their production. Five different heat storage layouts are investigated for integration in the overall system: three of them are direct-type tank-based units (Fig. 7), namely a fully mixed storage tank, a stratified storage tank and a two tank design with variable volume; the remaining two are a sensible packed bed and a latent packed bed (Fig. 8). Note that Fig. 7 and Fig. 8 refer to the steam generation scenario only. In the electricity scenario the steam generator is replaced by a power block.

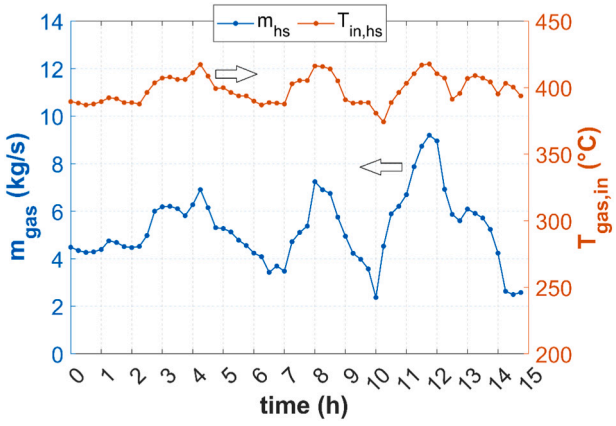

Fig. 6. Variation of the mass flow rate and temperature of the flue gas of a steel billet reheating furnace (taken from [16]) selected as waste heat source in this work.

3. Results

3.1. Preliminary design of the heat storage

In this Section the results obtained by the application of the initial steps of algorithm to the case study are shown. The presentation of the results follows the same numbering of the steps in the flowcharts of Fig. 2 and Fig. 3.

Step 1) The energy available from the flue gas is calculated from the profiles of Fig. 6 using a sampling time of 15 min. As shown in Table 7, the integration of a heat storage would enable the daily recovery of a significant amount of thermal energy (21.77 MWh), which otherwise would be wasted to the environment.

Step 2) Table 8 shows the selected functional parameters for the three storage categories. Considering sensible heat storage, the minimum temperature of 200 °C would enable the generation of steam with the required thermodynamic parameters (7 bar(a) and 180 °C) throughout the discharging process. On the other hand, the selection of a maximum temperature of 350 °C implies a quite significant ΔT equal to 150 °C. A melting temperature of 220 °C is selected as functional parameter of the latent heat storage to account for any temperature drop implied by the intermediate HTF between PCM and steam. As for the thermochemical storage, the reaction temperature is selected equal to 250 °C, taking into account that the temperature of the synthesis reaction (discharging) is typically lower than that of the decomposition reaction (charging) to ensure proper reaction kinetics.

Step 3) According to the selected functional parameters, the fraction of available heat which can be recovered by the storage system can be preliminarily estimated. Table 9 shows that charging efficiencies in the range 60–80% are obtained, which can be considered satisfactory. It is important to note that the charging efficiencies calculated at this step are only rough estimates, any dynamic aspect of storage being neglected.

Step 4) The application of the fourth step is illustrated using a limited set of storage materials in the database:

- Sensible storage media. All the considered solids can operate in the selected interval 200–350 °C (Fig. 9a). On the other hand, the use of

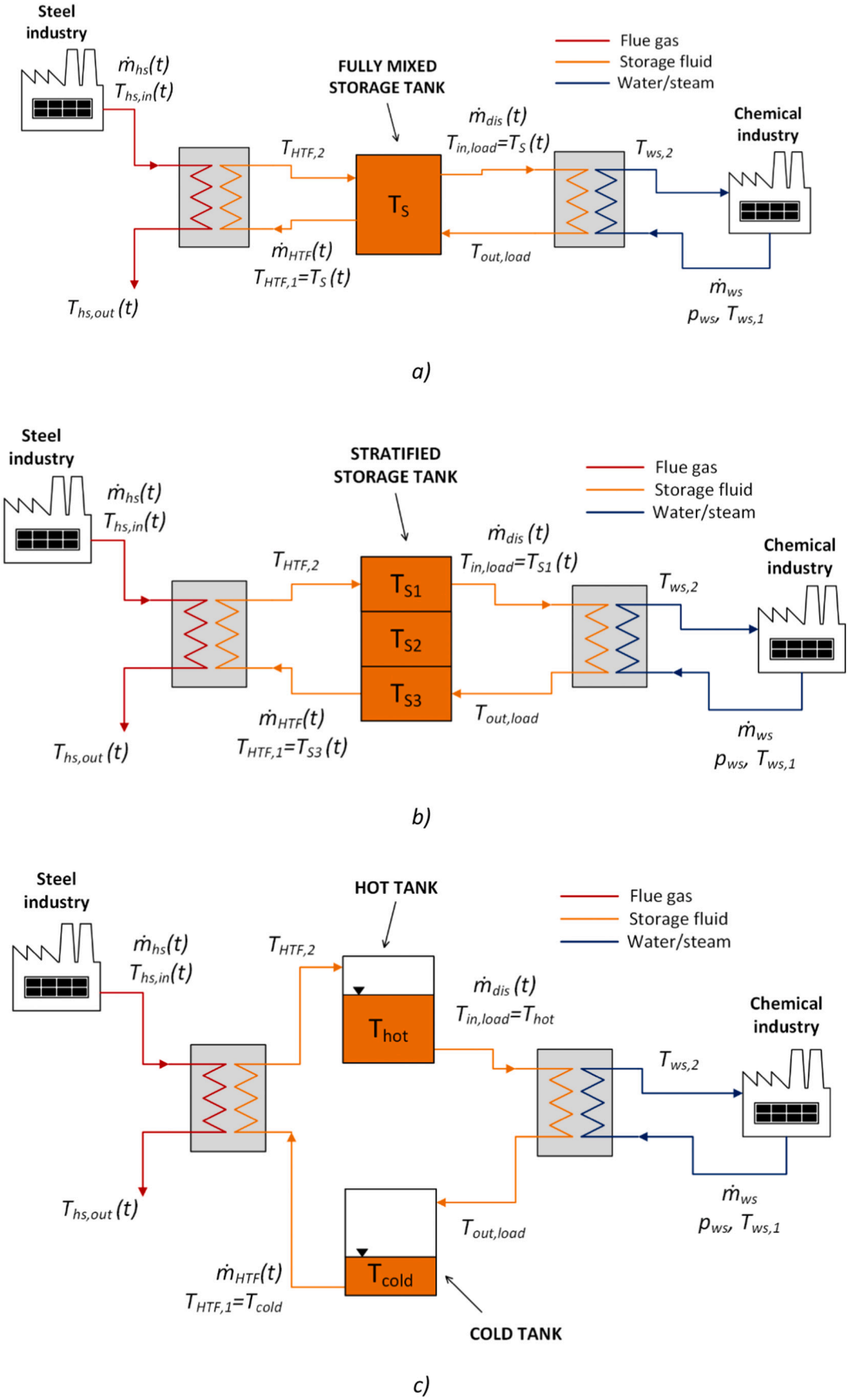

Fig. 7. Integration of tank-based storage units for the recovery of industrial waste heat and generation of process steam: a) fully mixed storage tank; b) stratified storage tank; c) two tank storage.

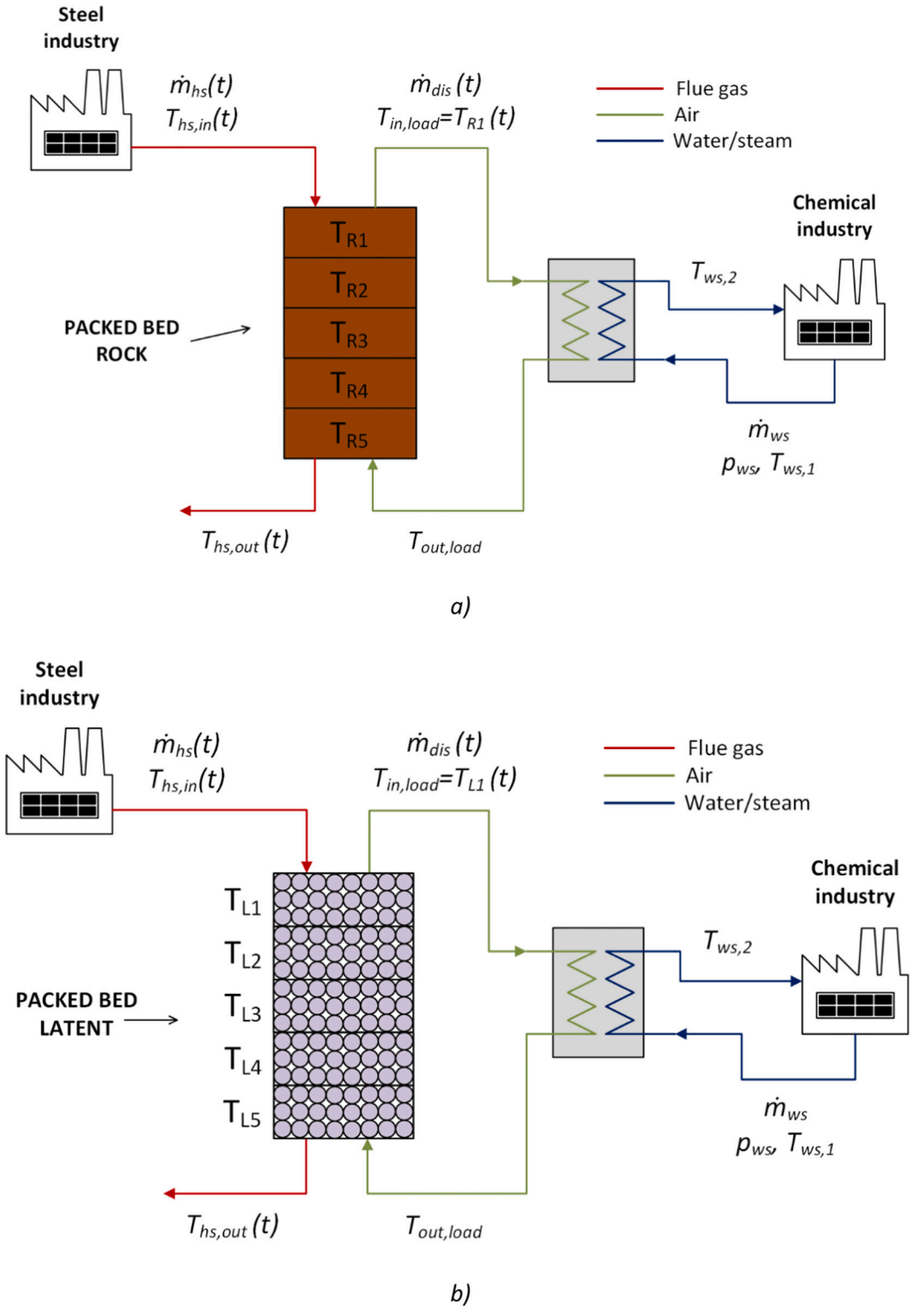

Fig. 8. Integration of packed bed based storage units for the recovery of industrial waste heat and generation of process steam: a) sensible packed bed using rock as filling material; b) latent packed bed using PCM as filling material.

certain liquid media (e.g. mineral oil, nitrite salts) may narrow this temperature range (Fig. 9b). Also, some liquid media (water and carbonate salts) are not viable for the considered application.

- Latent storage media. Different types of PCMs (organics, pure molten salts and salt mixtures, metallics) with melting temperatures in the proximity of the selected melting temperature are shown in Fig. *10*a, where the temperature bands account for the various values reported in the literature. Besides $NaNO_3$-KNO_3, which closely matches the selected melting temperature, other two molten salt mixtures ($NaNO_3$-NaOH and LiCl-LiOH) with higher melting temperatures are shortlisted.
- Thermochemical storage media. Different types of TCMs (zeolites, hydroxides, carbonates, hydrides, organics) with reaction temperatures in the proximity of the selected reaction temperature are shown

Table 7
Application of step 1 of the algorithm: calculation of the waste heat available.

Parameter	Symbol	Value
Inlet temperature flue gas	$T_{in,hs}$	See profile in Fig. 6
Mass flow rate flue gas	$\dot{m}_{hs}$	See profile in Fig. 6
Specific heat flue gas	$c_{p,hs}$	1.1 kJ/kg-K
Minimum outlet temperature flue gas	$T_{out,min,hs}$	150 °C
Charging time	t_{ch}	15 h
Sampling time	Δt	15 min
Heat available from the waste heat source	$Q_{hs,av}$	78,370 MJ (21,770 kWh)

Table 8
Application of step 2 of the algorithm: selection of the functional parameters.

Storage category	Parameter	Symbol	Value
Sensible	Minimum storage temperature	$T_{min,S}$	200 °C
	Maximum storage temperature	$T_{max,S}$	350 °C
Latent	Melting temperature	T_{melt}	220 °C
Thermochemical	Reaction temperature	T_{react}	250 °C

Table 9
Application of step 3 of the algorithm: preliminary calculation of the charging efficiency.

Storage category	Parameter (Symbol)	Value
Sensible	$Q_{S,ch}$	62,740 MJ (17,430 kWh)
	η_{ch}	80.1%
Latent	$Q_{S,ch}$	56,490 MJ (15,690 kWh)
	η_{ch}	72.1%
Thermochemical	$Q_{S,ch}$	47,120 MJ (13,090 kWh)
	η_{ch}	60.1%

in Fig. *10*b. A quite large band of charging temperatures is reported for each TCM due to the different operating conditions (mainly pressure) of different studies in the literature. Various materials (e.g. magnesium hydroxide) match the targeted charging temperature.

In spite of the availability of suitable materials in all the storage categories, the following analysis will focus on the sensible and latent storage media only, which appear the most obvious options for the considered short term thermal energy storage.

Step 5) In the fifth step a simple additive weighting method (see Appendix A) is used for the ranking of the storage materials, where the weights are assigned by the algorithm's user [28]. The choice of the attributes is shown in the following to be dependent on the type of heat storage.

- Solid media. The attributes considered are density, specific heat, heat conductivity and specific cost. According to the assumed importance weights, the solid material achieving the highest total score is sand/rock used in packed bed systems (Table 10).

- Liquid media. Table 11 shows the density and specific heat of the liquid materials potentially suitable for the application along with their temperature range.

Since the operating temperature ranges of some liquid media cover only partially the selected temperature range 200–350 °C, the energy density per unit of mass ($E_{d,M}$) and energy density per unit of volume ($E_{d,V}$), which include the temperature difference in their expressions, were used as attributes:

$$E_{d,M} = c_{p,m} \cdot \Delta T \tag{18}$$

$$E_{d,V} = \rho_m \cdot c_{p,m} \cdot \Delta T \tag{19}$$

In addition, the preliminary estimate of charging efficiency was used as further attribute, to account for the reduction of the utilization of the flue gas resulting from minimum material temperatures higher than 200 °C. The thermal conductivity and the specific cost complete the list of attributes. Table 12 shows that, under the assumed weights, the highest score is achieved by silicone oil.

- Phase change media. The attributes used for the ranking of the PCMs are the latent heat of fusion, the mass density and the thermal conductivity as well as the preliminary evaluation of the charging efficiency and the specific cost. In spite of its moderate latent heat of fusion, the highest score, given the assumed importance weights, is reached by the salt mixture $NaNO_3$-KNO_3 (Table 13).

Step 6) The mass, volume and material cost of the heat storage units calculated for the highest ranked materials are shown in Table 14. It clearly appears that the solid storage is the cheapest option, followed by the PCM storage. On the other hand, the silicone oil could be replaced by the cheaper mineral or synthetic oil in the search for a cost effective liquid storage system. However, it must be highlighted that the media costs in Table 14 can orientate the selection of a storage medium, but they do not include the often major costs of containers and heat exchanger equipment.

Step 7) Table 15 shows the storage layouts and the dynamic simulation models selected for the three storage materials. Three different layouts are considered for the liquid storage, namely a fully mixed tank, a stratified tank and a two tank storage, whose simulation models are

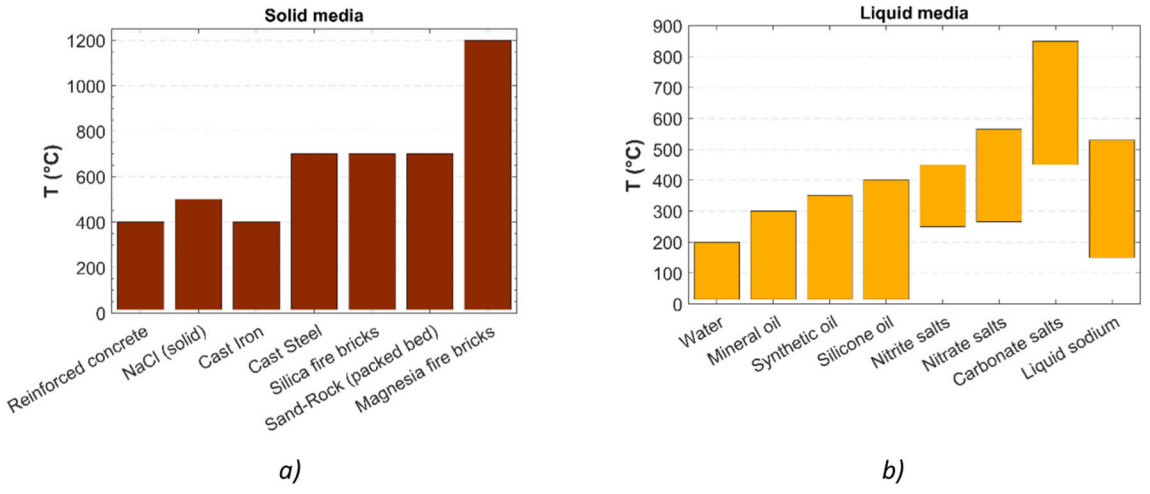

Fig. 9. Operating temperature ranges of sensible storage materials: a) solid media; b) liquid media.

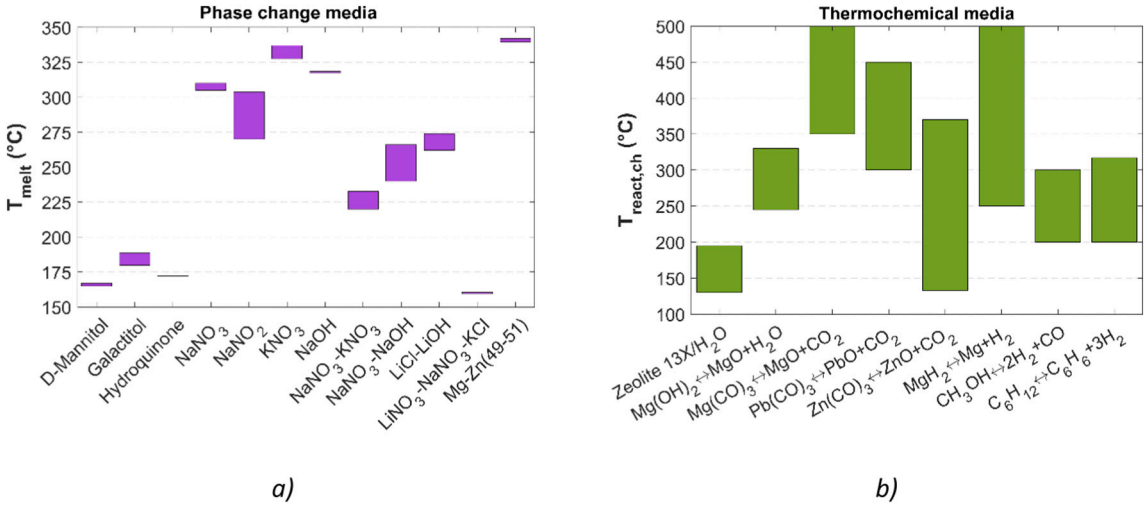

Fig. 10. Operating temperatures of phase change and thermochemical materials potentially suitable for the considered application: a) melting temperature of phase change materials; b) charging reaction temperature of thermochemical materials.

Table 10
Application of step 5 of the algorithm: scores achieved by the solid media and ranking.

Solid media	ρ_m (kg/m^3)	$c_{p,m}$ (kJ/kg-K)	λ_m (W/m-K)	c_m (€/kg)*	Total score	Ranking
Reinforced concrete	2200	0.85	1.5	0.08	0.479	4
NaCl (solid)	2160	0.85	7.0	0.25	0.366	6
Cast Iron	7200	0.56	37.0	1.7	0.512	3
Cast Steel	7800	0.60	40.0	8.4	0.544	2
Silica fire bricks	1820	1.0	1.5	1.7	0.315	7
Sand-Rock-Air (packed bed)	1500	1.0	0.5	0.05	0.613	1
Magnesia fire bricks	3000	1.15	5.0	3.4	0.395	5
Weights	6	8	5	9	/	/
Normalized weights	0.214	0.286	0.179	0.321	/	/

* updated from [29] using a CEPCI ratio = 1.88 and a currency conversion rate 1$ = 0.9€.

Table 11
Properties of the liquid media and temperature range of utilization for the case study considered.

Liquid media	ρ_m (kg/m^3)	$c_{p,m}$ (kJ/kg-K)	T_{min} (°C)	T_{max} (°C)	ΔT (°C)
Mineral oil	770	2.6	200	250*	50
Synthetic oil	900	2.3	200	300*	100
Silicone oil	900	2.1	200	350	150
Nitrite salts	1825	1.5	250	350	100
Nitrate salts	1870	1.6	265	350	85
Liquid sodium	853	1.3	200	350	150

* the maximum temperature was conservatively set 50 °C lower than the maximum admissible temperature.

well established (see e.g. [30,31]). The selected layout for both the solid storage and the PCM storage is the packed bed, which enables an effective stratification and, in turn, an effective heat extraction from the waste heat source. The corresponding simulation models are a simple equilibrium model for the packed bed rock storage [32], and a separate phases model first developed in [33] for the PCM storage.

3.2. Performance evaluation

3.2.1. Dynamic thermal response during charging (application of step 8 of the algorithm)

This Section shows the results obtained by the application of the eighth step of the algorithm (see Fig. 4) to the case study. In-house simulation models have been developed in Engineering Equation Solver (EES) for all storage types. The simulation results obtained for the tank based storage units have been successfully validated against an established commercial software (TRNSYS) using the same forcing function. The simulation results obtained for the packed bed sensible and latent heat storage units have been validated against experimental data in the literature. The validation confirms and ensures that predictions of the proposed models are reliable for the intended study presented in this manuscript, as shown in the next two paragraphs.

3.2.1.1. Validation of the sensible packed bed storage model against experimental data. The results obtained from the developed simulation model of packed bed sensible storage are herein compared against the experimental results for a commercial unit, originally shown in [34] and later reported in [35], for model validation. The main characteristics of the packed bed are summarized in Table 16, whereas Table 17 shows the test data.

Thirteen thermocouples evenly spaced along the flow path within the pebble-bed were used in [34] to obtain the grey lines shown in the background of Fig. 11 for a typical charging test. The pebble-bed showed a large degree of stratification as evidenced by the shape of the curves in the first hours of the test. The time variation of the fluid temperatures obtained by our simulation model are shown as coloured dashed lines in Fig. 11. By comparing the simulation results against the measured temperatures it can be noticed that the simulation model predicts higher fluid temperatures, a lower degree of stratification and faster charging times. In spite of these deviations the model validation can be considered satisfactory for the scope of this work. For a higher accuracy the storage model could be upgraded to a non-equilibrium model (see e.g. [36]).

3.2.1.2. Validation of the latent packed bed storage model against experimental data. In [33] the experimental measurements of transient temperature distributions in a randomly packed bed of uniform spheres containing a PCM for a step-change in inlet air temperature are reported. The packing was composed of spheres filled with paraffin wax. Temperatures of the PCM and air were measured at seven axial locations at

Table 12
Application of step 5 of the algorithm: scores achieved by the liquid media and ranking.

Liquid media	$E_{d,M}$ (kJ/kg)	$E_{d,V}$ (MJ/m^3)	η_{ch} (%)	λ_m (W/m-K)	c_m (€/kg)	Total score	Ranking
Mineral oil	130	100	80.1	0.12	0.51	0.597	3
Synthetic oil	230	207	80.1	0.11	5.1	0.562	4
Silicone oil	315	284	80.1	0.10	8.4	0.680	1
Nitrite salts	150	274	60.1	0.57	1.7	0.561	5
Nitrate salts	136	254	54.1	0.52	1.2	0.547	6
Liquid sodium	195	166	80.1	71	3.4	0.623	2
Weights	8	9	7	4	8	/	/
Normalized weights	0.222	0.250	0.194	0.111	0.222	/	/

Table 13
Application of step 5 of the algorithm: scores achieved by the phase change media and ranking.

Phase change media	ΔH_{melt} (kJ/kg)	ρ_{PCM} (kg/m^3)	λ_{PCM} (W/m-K)	η_{ch} (%)	c_{PCM} (€/kg)	Total score	Ranking
$NaNO_3$-KNO_3	107	1980	0.59	71.3	0.26	0.749	1
$NaNO_3$-NaOH	206	2180	0.63	60.2	0.35	0.721	2
LiCl-LiOH	430	1550	1.1	53.7	17.4	0.671	3
Weights	8	6	7	9	9	/	/
Normalized weights	0.205	0.154	0.179	0.231	0.231	/	/

Table 14
Application of step 6 of the algorithm: preliminary calculation of storage mass, volume and material cost.

Type of storage	Sensible		Latent
Storage media	Silicone oil	Rock-Sand-Air	$NaNO_3$/KNO_3
Heat charged (MJ)	62,740	62,740	55,870
Mass (tons)	199.2	418.3	521.2
Volume (m^3)	221.3	278.9	263
Media cost (k€)	1673	20.9	135.5

Table 15
Application of step 7 of the algorithm: selection of the storage layout and model.

Type of storage	Sensible		Latent
Storage media	Silicone oil	Rock-Sand-Air	$NaNO_3$/KNO_3
Layout of storage	1) Fully mixed 2) Stratified tank 3) Two tank	Packed bed	Packed bed
Model of storage	1) Constant mass and uniform T 2) Constant mass multinode using three nodes 3) Variable mass/ volume	One dimensional equilibrium model using five layers	Separate phases one dimensional model using five layers

Table 16
Design features of the sensible packed bed used for model validation.

Parameter	Value	Unit
Bed height	1.8	m
Bed cross sectional area	$2 \times 2 = 4$	m^2
Packing material	Gravel	/
Particle diameter	0.038–0.05	m
Particle density	1538	kg/m^3
Particle specific heat	880	J/kg-K
Mean void fraction*	0.35	/

* Estimated.

Table 17
Pebble bed test data used for model validation.

Parameter	Value	Unit
Charging time	5.42	h
Air flow rate	0.495	kg/s
Initial temperature	24.2	°C
Input temperature	60.1	°C
Heat loss	13.9	MJ
Loss heat transfer coefficient	2.3	W/m^2-K
Effective thermal conductivity	0.26	W/m-K

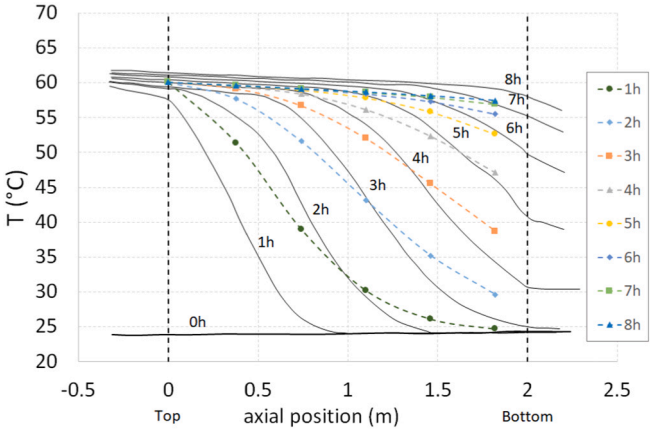

Fig. 11. Variation of the fluid temperature with the axial position along the packed bed for different times. Grey lines: experimental data reported in [34]; coloured dashed lines: results of the simulation model using five nodes.

Table 18
Characteristics of the experimental bed tested in [33] used for model validation.

Parameter	Value	Units
Bed length	0.278	m
Bed diameter	0.208	m
Particle diameter	0.0201	m
Average particle density	811.8	kg/m^3
Effective solid specific heat	8.374	kJ/kg-K
Effective liquid specific heat	2.093	kJ/kg-K
Average PCM conductivity	0.2406	W/m-K
Effective latent heat of fusion	197.7	kJ/kg
Mean void fraction	0.369	/

Table 19
Operational parameters either reported in [33] or calculated used for model validation.

Parameter	Value	Units
Mass flow rate of air	0.0328	kg/s
Inlet temperature of air	≈60	°C
Re_0	970	/
Pr	0.7207	/
Nu	99	/
U	134.8	W/m^2-K
U_{eff}	66.0	W/m^2-K

the centreline of the bed. Table 18 lists the characteristics of the experimental bed, whereas Table 19 reports the test data as either reported in [33] or calculated.

The time variations of the PCM temperature predicted (black lines) and measured (orange marks) at two axial locations in [33] are shown in Fig. *12*a. Instead, the results obtained using our simulation model are shown in Fig. *12*b, where the black lines refer to the predicted PCM temperature at five nodes (i.e., evenly spaced axial positions) and the orange marks refer again to the measured data. It clearly appears from the comparison that our simulation model predicts quite well the charging time at any axial location. The measured charging time is higher than that predicted by our model by approximately 0.2 h, however this difference can be considered satisfactory for the scope of this work.

3.2.1.3. Transient response of fully mixed, stratified and two tank layouts using oil as storage medium. Fig. 13 shows the transient thermal response during charging for the three tank based storage units, namely fully mixed, stratified and two tank, using silicone oil as storage medium. The plots show the time variation of the storage temperature, the flue gas temperature at the outlet of the gas-to-oil heat exchanger and the instantaneous charging efficiency. The initial temperature of the storage medium is 200 °C for the fully mixed and stratified tank, which is the minimum storage temperature assumed in the preliminary design. In the two tank layout the initial temperatures of the cold and hot tanks are 200 °C and 300 °C, respectively. The volume of silicone oil is constant in the fully mixed and stratified tank and it is assumed equal to 220 m^3, from the preliminary design calculations. In the gas-to-oil heat exchanger the thermal oil is heated up to a set point temperature of 350 °C.

The dynamic response in the charging process is highly dependent on the storage layout:

- Fully mixed storage (Fig. 13a). The gradual increase of the (uniform) storage temperature is accompanied by a similar increase of the flue gas outlet temperature. Indeed, the rising temperature of the thermal oil exiting the storage tank and entering the gas-to-oil heat exchanger hinders the extent of cooling of the heat source. Accordingly, the instantaneous charging efficiency gradually decreases. In the second part of the charging process less than half of the thermal power available from the heat source is transferred to the heat storage.
- Stratified storage (Fig. 13b). The bottom layer of thermal oil remains at a much lower temperature compared to the top layer throughout the charging process. In particular, in the first half of charging the temperature of the bottom layer remains close to the minimum storage temperature. Since the oil stream entering the gas-to-oil heat exchanger is withdrawn from the bottom layer, the heat extraction from the flue gas significantly improves compared to the fully mixed tank. Nevertheless, the instantaneous charging efficiency still deteriorates towards the end, due to the marked temperature increase of the bottom layer.
- Two tank storage (Fig. 13c). The temperature of the thermal oil entering the gas-to-oil heat exchanger from the cold tank is approximately constant. The admission of hot silicone oil in the hot tank increases the volume as well as the temperature of the storage material in the hot tank. The flue gas temperature at the outlet of the gas-to-oil heat exchanger remains at the minimum level throughout the entire charging. Accordingly, the instantaneous charging efficiency does not deteriorate as the charging progresses, the small fluctuations being due to the fluctuation of the heat source inlet temperature.

By integrating the instantaneous charging efficiencies over the duration of the charging process, it is possible to compare the behaviour of the three storage layouts on the basis of a global value, namely the charging efficiency. The latter was calculated equal to 49.7% for the fully mixed tank, 59.7% for the stratified tank and 68.1% for the two tank design, which demonstrates the importance of the selection of the heat storage configuration, beside the storage material, in capturing the industrial waste heat.

3.2.1.4. Transient response of the packed bed layout using rock or PCM as storage material. The transient thermal responses during charging for the packed bed layouts using either rock or encapsulated molten salt ($NaNO_3/KNO_3$) are shown in Fig. 14. By combining the indications from the preliminary sizing and costing with the analysis of the dynamic

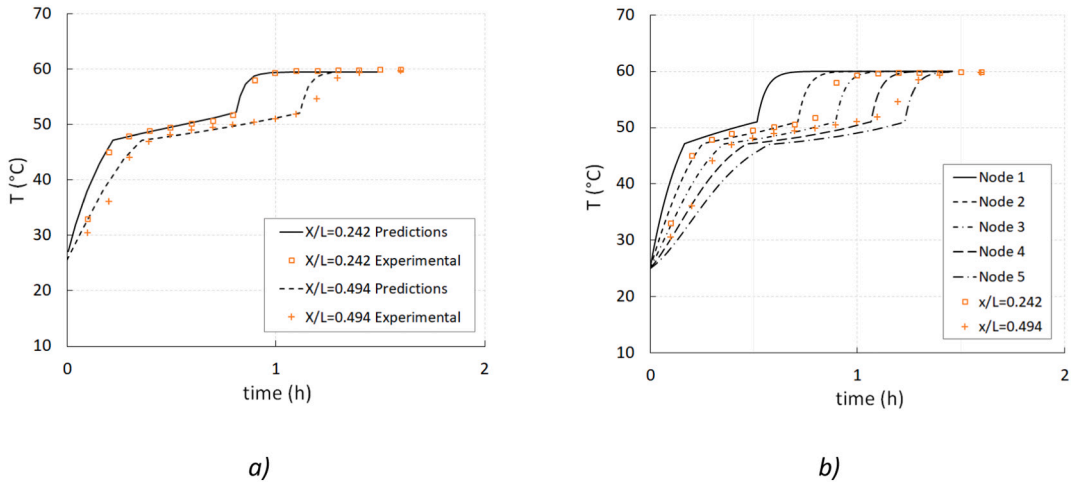

Fig. 12. Time variation of the PCM temperature versus time: a) temperature at two axial positions (x/L = 0.242 and x/L = 0.494) measured and predicted in [33]; b) temperature at five axial positions (nodes) obtained by our simulation model (black lines) and comparison against the experimental results (orange marks) obtained in [33].

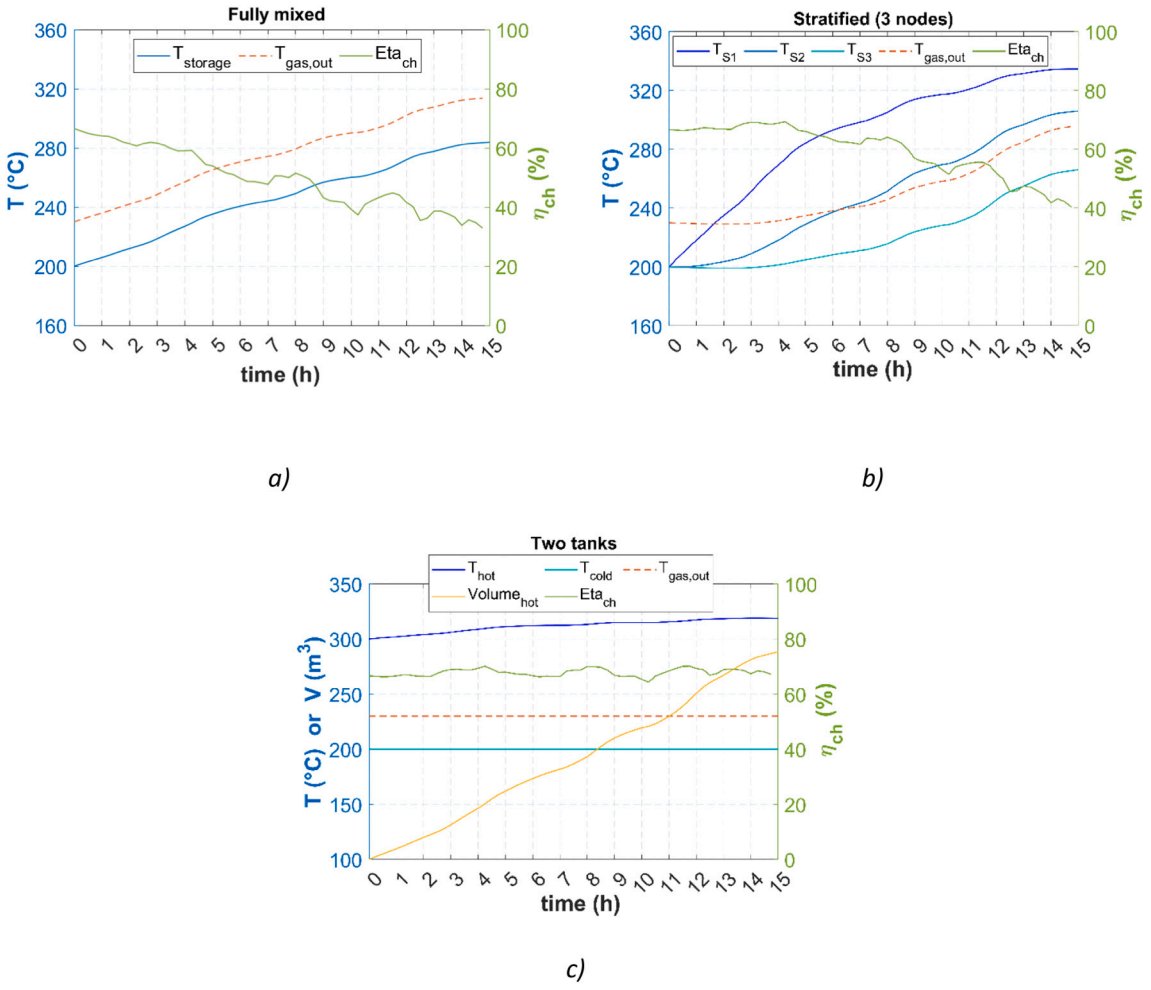

Fig. 13. Transient thermal response of three types of sensible heat storage using silicone oil as storage medium during the charging process: a) fully mixed tank; b) stratified tank; c) two tank storage.

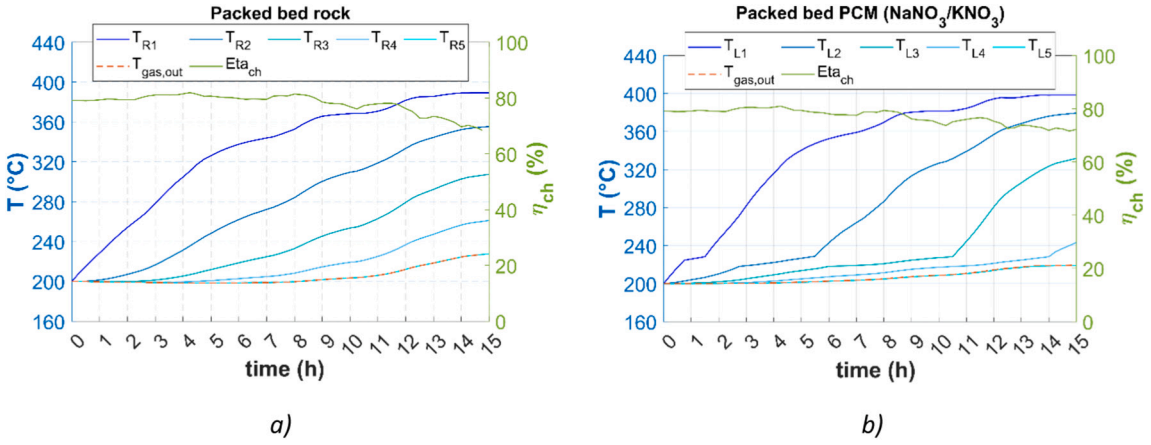

Fig. 14. Transient thermal response of packed bed systems during the charging process: a) sensible packed bed using rocks as packing material; b) latent heat packed bed using encapsulated solar salt.

response obtained by running some initial simulations, the volume of the rock bed was increased to 400 m^3, whereas the volume of the PCM bed was set at 200 m^3. The increase of the rock bed volume (from 279 to 400 m^3) leverages on the cheap rock material, whereas the decrease of the latent storage volume (from 263 to 200 m^3) targets volume constrained applications. For both units the initial temperature of the storage material was 200 °C, for a fair comparison with the tank based layouts.

Due to the punctual contact between bed particles, both the sensible and latent packed bed layouts lead to an effective thermal stratification, as described below:

- Packed bed rock (Fig. 14a). When after 9 h of charging the temperature of the top rock layer has almost approached the maximum temperature, the temperature of the bottom layer is still stuck to the minimum value. Accordingly, the outlet temperature of the flue gas leaving the packed bed, which is in equilibrium with the bottom layer, is kept very low throughout the charging process. Due to the effective stratification and the direct heat transfer between flue gas and storage material, the instantaneous charging efficiency remains high, around 80%, for most of the charging time.
- Packed bed PCM (Fig. 14b). The temperature profiles of the different layers of PCM clearly show the solid-liquid phase change transition. The time duration of the phase change process increases while moving from the top layer to the bottom layer, due to the reduction of the flue gas temperature when crossing the packing bed. At the end of the charging process, the bottom layer is still experiencing phase transition. The flue gas leaves the packed bed at temperatures lower or close to the melting temperature of $NaNO_3/KNO_3$, which implies high values of the instantaneous charging efficiency.

The calculated charging efficiencies are 78.3% and 77.4% for the packed bed rock and packed bed PCM layout, respectively. Both of them are higher than the tank based storage units. It is also noteworthy that

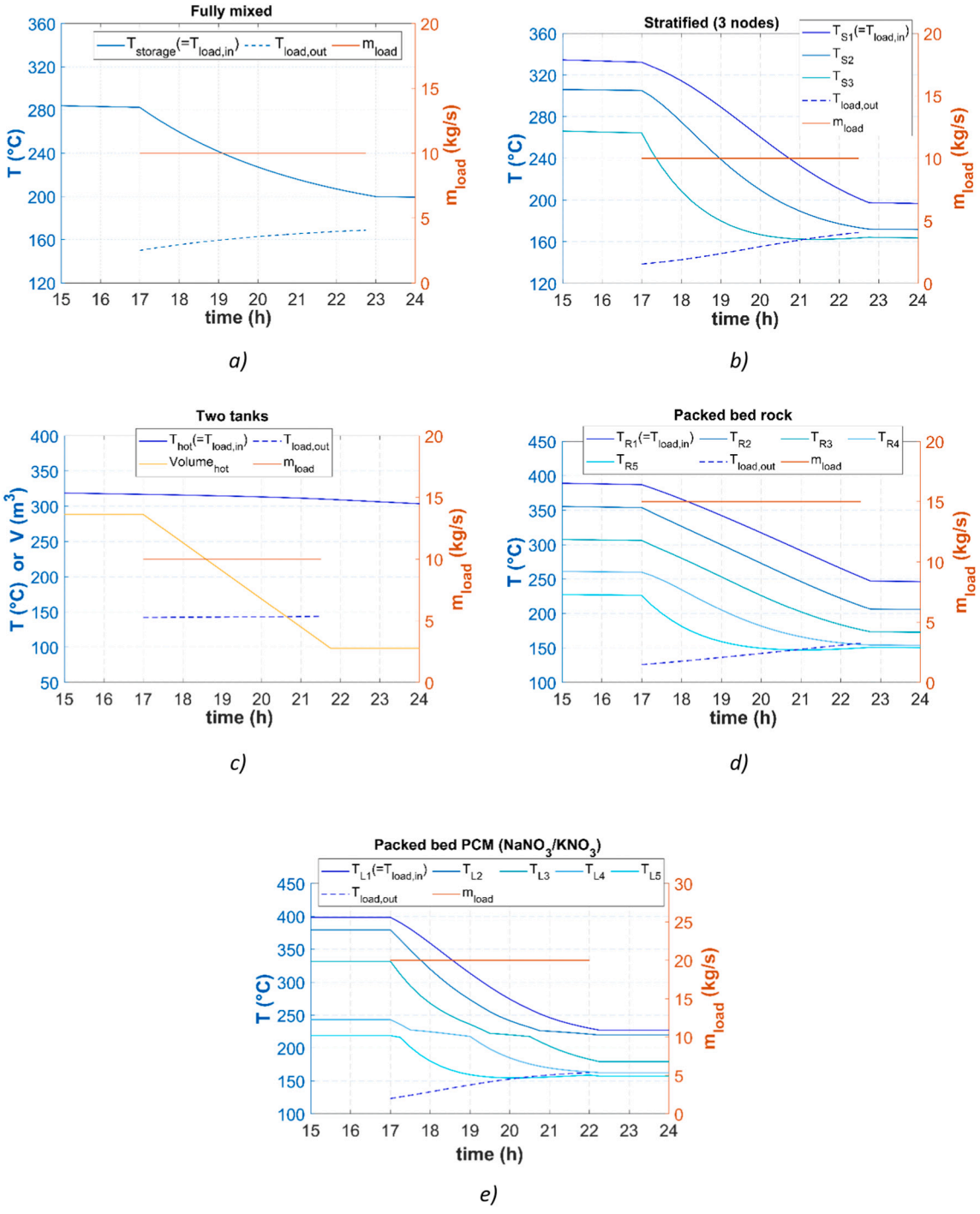

Fig. 15. Transient thermal response of the thermal energy storage during the discharging process: a) fully mixed tank; b) stratified tank; c) two tank storage; d) packed bed rock; e) packed bed PCM.

the PCM storage can capture and store approximately the same amount of heat as the rock storage while using only half volume.

3.2.2. Dynamic thermal response during discharging with steam production (step 9 of the algorithm)

3.2.2.1. Transient response of tank based layouts and packed bed layouts. This Section shows the results obtained by the application of the ninth step of the algorithm (Fig. 5) to the case study with steam generation. The dynamic thermal responses of the five different storage layouts during the discharging process are presented in Fig. 15. After an idle period of 2 h, the discharging is assumed to start at hour seventeen and to end when the storage parameters reach a given condition. The mass flow rate of heat transfer fluid exiting the storage tank and entering the steam generator is assumed constant (10 kg/s for the tank based layouts, 15 kg/s for the packed bed rock and 20 kg/s for the packed bed PCM) throughout the discharging process. Different mass flow rates were used due to the different heat transfer fluid properties (oil, air) and storage designs so that the storages are fully discharged before hour 24. The thermal power transferred in the heat exchanger is used to raise superheated steam at 7 bar and 180 °C from condensate water returned at 50 °C.

The dynamic thermal response varies depending on the storage layout and material, as described below:

- Fully mixed tank (Fig. 15a). The oil temperature in the tank and, identically, the temperature of oil entering the steam generator gradually decrease as the time progresses. The discharging process ends when the storage temperature reaches the threshold temperature of 200 °C. Conversely, the return oil temperature slightly increases, as from the energy balance in the steam generator. As a result, the mass flow rate of raised steam progressively declines due to the reduction of the temperature difference of thermal oil in the heat exchanger.
- Stratified tank (Fig. 15b). The temperature of the upper node and, identically, of the oil entering the steam generator are much higher than the temperature of the fully mixed tank throughout the discharging process. This results in a much higher heat load in the heat exchanger and, in turn, a higher mass flow rate of raised steam. The discharging continues as long as the temperature of the upper layer is higher than the threshold temperature.
- Two tank storage (Fig. 15c). The temperature of the hot tank and, likewise, of the oil entering the heat exchanger remain almost constant. This implies almost constant trends of the return oil temperature as well as of the mass flow rate of raised steam. The discharging process ends when the volume of the hot tank has reached the minimum value.
- Packed bed rock (Fig. 15d). Due to the effective stratification, the temperature of the upper rock layer, which is equal to the temperature of the air flow entering the steam generator, remains much higher than the other layers throughout the discharging process. This, combined with the low air return temperature, implies a high heat transfer rate in the steam generator. The discharging is assumed to end when the temperature of the upper layer reaches 250 °C.
- Packed bed PCM (Fig. 15e). Even though the liquid-solid phase transition process is characterized by quasi-horizontal segments, the air temperature exiting the storage follows the temperature profile of upper PCM layer, which remains in the liquid state throughout the discharging. It is indeed assumed that the discharging ends when the upper layer reaches the freezing point. Similarly to the packed bed rock, the discharging is characterized by a high transfer rate in the steam generator.

3.2.2.2. Steam generated in the discharging process. Fig. 16 compares the amount of steam raised in the discharging process for all the considered

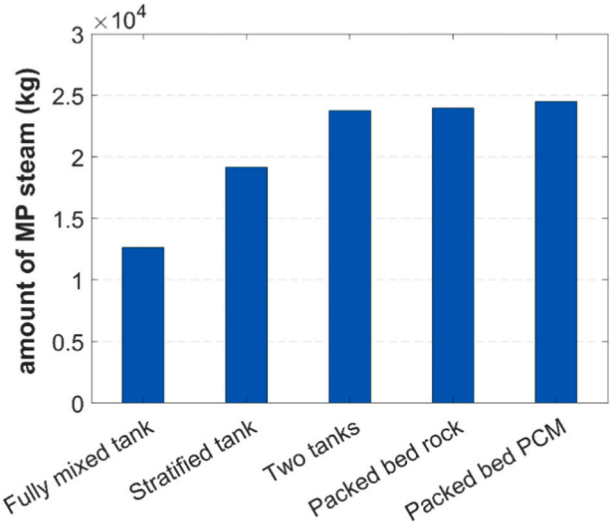

Fig. 16. Amount of medium pressure steam generated in the discharging process: comparison between different heat storage options.

storage options. Focusing on thermal oil, it clearly appears that the stratified tank and the two tank layouts lead to a much higher steam production compared to the fully mixed tank. This is the effect of a higher charging efficiency combined with a higher temperature level of the heat stored and transferred to the steam generator. In particular, the amount of steam obtained using the two tank layout is almost double than that employing a fully mixed storage. With regards to the packed bed layout, there are not significant differences in terms of steam production between the sensible and the latent heat storage, because both systems achieve similar charging efficiencies and high temperatures of the stored heat.

3.2.3. Dynamic thermal response during discharging with electricity generation (step 9 of the algorithm)

The ninth step of the algorithm is applied in this section to the same case study, but considering the electricity generation scenario. The dynamic thermal response during discharging is evaluated using the previous storage simulation models along with input-output performance models developed for different heat-to-power systems. Fig. 17 shows a schematic of the overall heat recovery system with electricity generation, considering a fully mixed storage tank and a generic power block. Similar schematics can be drawn for the other storage types by adapting the corresponding schematics of Fig. 7 and Fig. 8.

3.2.3.1. Performance models of waste heat to power systems. Fig. 18 shows the performance correlation curves of four heat-to-power systems obtained in this work from a literature survey and used as block-box models at the ninth step of the algorithm. For each heat-to-power technology the trends of two performance metrics, namely the thermal efficiency (η_{th}) and the heat recovery effectiveness (ε_{hr}), are shown as a function of the inlet temperature of the heat transfer fluid entering the power block. The thermal efficiency is the ratio between the net power output and the heat input (i.e. the heat transferred) to the power cycle:

$$\eta_{th} = \frac{\dot{W}_{net}}{\dot{Q}_{in}} = \frac{\dot{W}_{net}}{\dot{m}_{HTF} \cdot c_{p,HTF} \cdot (T_{in} - T_{out})_{load}} \tag{20}$$

The heat recovery effectiveness is the ratio between the heat transferred to the power cycle and the overall heat available from the inlet temperature to the ambient temperature:

$$\varepsilon_{hr} = \frac{\dot{m}_{HTF} \cdot c_{p,HTF} \cdot (T_{in} - T_{out})_{load}}{\dot{m}_{HTF} \cdot c_{p,HTF} \cdot (T_{in,load} - T_{amb})} = \frac{(T_{in} - T_{out})_{load}}{T_{in,load} - T_{amb}} \tag{21}$$

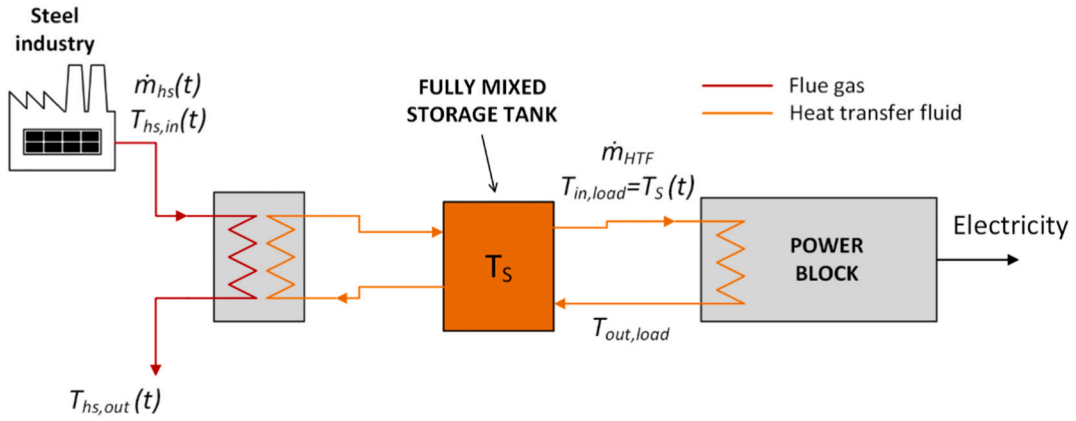

Fig. 17. Integration of a fully mixed storage tank for the recovery of industrial waste heat and generation of electricity.

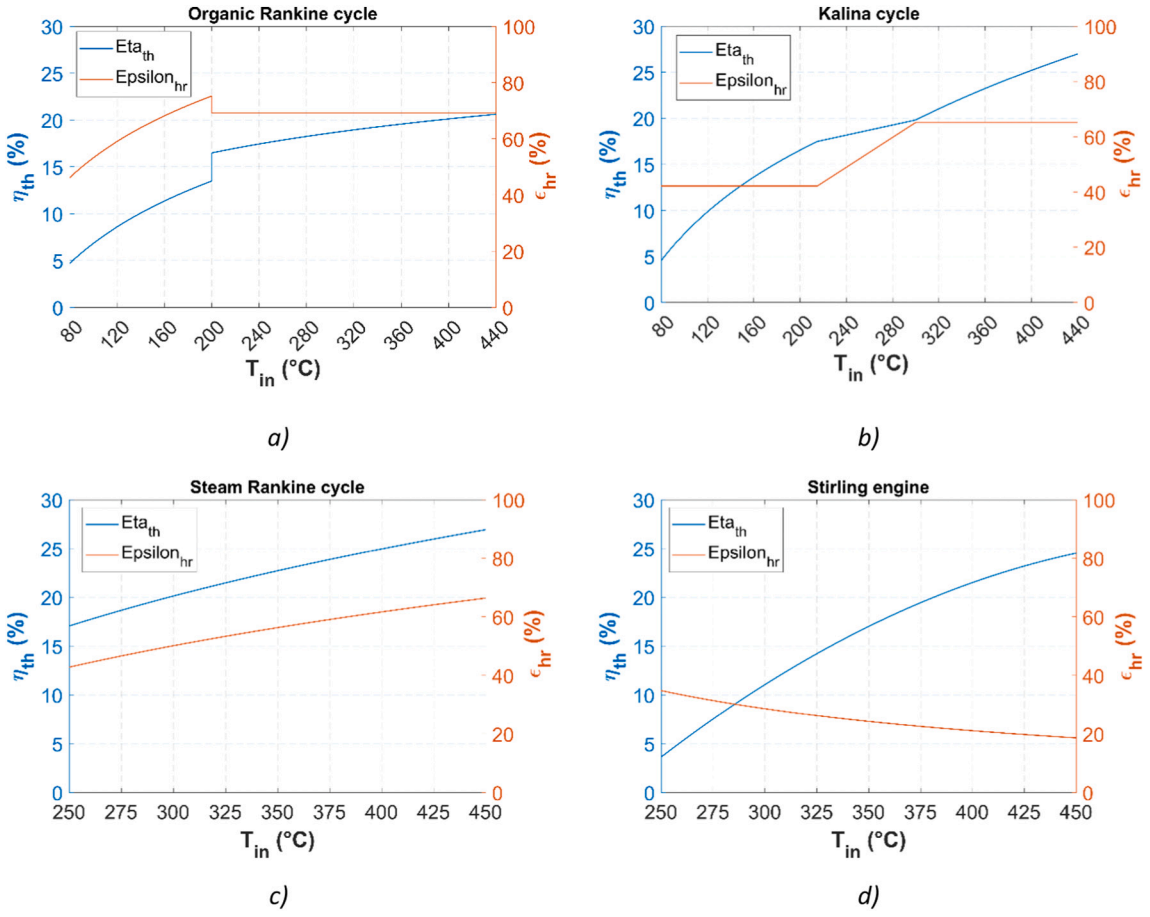

Fig. 18. Variation of thermal efficiency and heat recovery effectiveness as a function of the heat source inlet temperature for: a) low and medium/high temperature ORCs; b) low and medium temperature Kalina cycle; c) steam Rankine cycle; d) Stirling engine.

For given technology and inlet temperature, there are certain conditions of the internal thermodynamic parameters which lead to the maximum net power output. At these particular conditions, the couple thermal efficiency and heat recovery effectiveness assumes a single value, which is marked with the symbol "star":

$$\begin{cases} \eta_{th} \rightarrow \eta_{th}^{*} \\ \varepsilon_{hr} \rightarrow \varepsilon_{hr}^{*} \end{cases} \quad when\ \dot{W}_{net} \rightarrow \left(\dot{W}_{net}\right)_{max} \tag{22}$$

Fig. 18 shows only these optimum values of thermal efficiency and heat recovery effectiveness, which ultimately lead to the highest power output. The performance curves are the best fit curves obtained by considering and processing the results of several optimization studies reported in the scientific literature. The investigated temperature range in Fig. 18 is delimited between the minimum temperature of technical/economic viability of the technology and the maximum temperature of waste heat considered in this work. Due to the wide temperature range, some features of the heat-to-power technology may change (e.g. the cycle layout and/or the fluid), and this becomes evident in the discontinuity of either the values or the slope of the performance curves.

3.2.3.2. Electricity generated during the discharging step. The results summarized in the bar chart of Fig. 19 show that the electricity generated in the discharging process is dependent on both the heat storage type and the heat-to-power cycle. Indeed, each storage type exhibits a different dynamic thermal response and each power cycle features different performance curves. For any type of heat storage, the organic Rankine cycle (ORC) and the Kalina cycle (KC) appear the best technologies for electricity generation. For both the ORC and the KC the electricity generated increases by 65–70% if a stratified tank is used in place of a fully mixed storage tank, and almost doubles using a two tank layout. The packed bed layout, either of the sensible or latent type, combined with the ORC or KC yield the highest electricity in the range 4.0–4.2 MWh. The steam Rankine cycle (SRC) and the Stirling engine (SE) can be coupled with all the storage types except the fully mixed tank. In fact, the latter cannot provide the sufficient temperature (>250 °C) required for the operation of the SRC and SE throughout most of the discharging process. The SRC reaches a good performance only in combination with the two tank storage, due to the roughly constant temperature of the hot tank. Instead, when combined with the other storage types the electricity generated by the SRC is limited by the high threshold temperature. Finally, the Stirling engine cannot provide a satisfactory performance, which is four times lower than the best technologies.

3.2.4. Financial analysis and final selection of the storage unit (application of step 10 of the algorithm)

This Section shows the application of the tenth step of the algorithm which leads to the final storage selection. This is based on a financial analysis where the revenues deriving from selling steam or electricity are balanced against the costs of the storage units and the heat-to-power systems.

The investment cost of the storage system is estimated from the cost of storage material using the following equation:

$$C_{TES} = c_{SM/PCM/TCM} \cdot M_S \cdot f_1 \cdot f_2 \quad (23)$$

where c is the unit cost of the storage material (sensible, latent or thermochemical), M_S is the storage mass, f_1 is a multiplying factor which accounts for the cost of the other storage components (tank, insulation, blowers, heat exchangers, encapsulation material, etc.) along with their installation, f_2 is a multiplying factor which accounts for the indirect expenses (engineering, etc.).

The value of f_1(=2.7) for the tank-based storage was taken from the accurate feasibility study reported in [37], which showed the total storage cost and cost breakdown for synthetic oil and molten salt storage. The value of f_1(=10) for the sensible packed bed rock storage was taken from [38], which estimated that the rocks account for only 10% of the storage cost. The same value of multiplying factor f_1(=10) was assumed for the packed bed latent storage, also considering the costs reported in the literature for encapsulated PCM systems [39]. The multiplying factor f_2 was assumed 1.5 for the tank based storage, which is a consolidated technology, and equal to 3 for the packed bed sensible and latent storage, which are considered less mature. The O&M cost was simply assumed as 2% of the total storage cost. The specific investment cost (SIC) of the ORC was set at 3600 € per kW of installed power, and the O&M costs equal to 1.35 c€/kWh, as reported in [40] for a ORC capacity in the range 500 kW–1 MW. The same values were assumed for the KC due to the similar technology and cost data reported in the literature ([41,42]) for similar capacities.

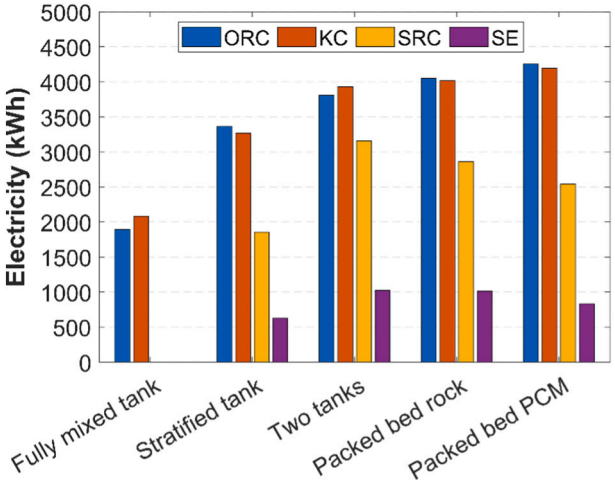

Fig. 19. Electricity generated during the discharging step for different combinations of heat storage type - heat engine: organic Rankine cycle (ORC), Kalina cycle (KC), steam Rankine cycle (SRC) and Stirling engine (SE).

As for the estimation of the revenues we used the average industrial price of natural gas in Europe throughout the first half of year 2021, which was 0.0303 €/kWh (0.44 €/kg) [43]. It is assumed that the steam generated during discharging displaces the steam generated in a natural gas boiler. In the electricity scenario, the electricity selling price was set to 10 c€/kWh. A plant life of 15 years, a number of 300 operating days per year and a discount rate of 5% complete the set of parameters used in the financial analysis.

The results obtained show that positive financial indicators are obtained when using the packed bed rock storage in the steam generation scenario. In this case, the payback time is 6.9 years, the net present value is 735 k€ and the internal rate of return reaches 15.5%. The economics worsen when the packed bed latent storage is considered due to the similar performance and the higher cost of the filling material. The tank based storage systems are found not profitable due to the high cost of the silicone oil. In the electricity scenario the integration of all storage options turned out to be not profitable due to the high investment cost and low utilization factor of the waste heat to power units. It is however worthy to emphasize that the economic scenario hinges on revenues coming exclusively from selling electricity. Further revenues streams might be actually accessible, particularly from the provision of some ancillary services through the generation assets considered (ORC, KC, etc) with flexibility provided by the thermal energy storage system. Nonetheless, such analysis it is beyond the scope of the work presented here. In conclusion, the packed bed rock unit is the most suitable option for this waste heat recovery application within a steam generation scenario. In the presence of constraints related to size of the storage the packed bed latent unit could be installed.

4. Conclusions

A structured procedure has been proposed in this work to broaden the spectrum of heat storage options and automatize their selection process in industrial waste heat recovery application. The selection is based on: i) the degree of heat extraction from the waste heat source in the charging process; ii) the amount of process steam or electricity generated in the discharging process; iii) the characteristics of the heat storage, like the volume and cost. By enlarging the boundaries of the analysis from the storage only to the overall system where the storage is integrated, a direct answer is obtained about the best heat storage selection. The structure of the proposed procedure, which is composed by a preliminary design stage followed by a performance estimation stage. Due to the underlying nature of the modeling methods, that is algebraic and one-dimensional models, the proposed methodology does not incur in significant computational costs. It can be performed on conventional hardware and thus support the screening of heat storage options whose dynamic behaviour is also assessed.

The procedure has been applied in this work to identify the best storage option for the recovery of a discontinuous flue gas at medium temperature in a steel industry. In spite of the limited number of storage materials and layouts considered at this stage, the outcome of the

methodology already leads towards less conventional storage options that are often overlooked. Indeed, it has been found that the selection of a packed bed heat storage, either of the sensible or latent type, results in the highest production of process steam in the discharging process. Moreover, the development and implementation of specific performance models for a set of heat-to-power technologies allowed to show that this also represent the best storage option for the conversion of waste heat into electricity, in combination with the organic Rankine cycle or the Kalina cycle. The financial analysis showed that the choice of a packed bed rock storage for the considered application results in a payback time of about seven years.

The developed methodology appears useful especially in the preliminary design stage where several heat storage options need to be considered. More accurate heat storage models can be used in a more advanced stage of the design for a precise evaluation of the overall performance.

CRediT authorship contribution statement

Giovanni Manente: Conceptualization, Methodology, Software, Formal analysis, Writing - original draft, Writing - review & editing, Visualization. **Yulong Ding:** Writing - review & editing, Funding acquisition. **Adriano Sciacovelli:** Conceptualization, Management, Writing - review & editing, Funding acquisition.

Declaration of competing interest

The authors declare that they have no known competing financial interests or personal relationships that could have appeared to influence the work reported in this paper.

Acknowledgements

This work was supported by the European Union's Horizon 2020 research and innovation programme (SO WHAT Project; grant number 847097).

Appendix A. Description of the multi-attribute decision making method (MADM) within STEP 5 of the algorithm

A.1. Presents the typical MADM performance matrix composed of m alternatives and n attributes, as well as the weights for every attribute.

Table A.1
MADM performance matrix.

	Attribute 1	Attribute 2	…	Attribute n
Material alternative 1	X_{11}	X_{12}	…	X_{1n}
Material alternative 2	X_{21}	X_{22}	…	X_{2n}
…	…	…	…	…
Material alternative m	X_{m1}	X_{m2}	…	X_{mn}
Attribute weights	W_1	W_2	…	W_n

The alternatives denote storage media candidates, while attributes refer to the quantitative (numerical) properties, such as specific heat, density, thermal conductivity, specific costs, etc. So X_{ij} from the matrix describes the value of property "j" possessed by material alternative "i". The weights determine the importance of each attribute relatively to each other, which are assigned by the engineer by a certain technique. Having the matrix available, engineers can thus run through a MADM algorithm to sort out the ranking. It is crucial to apply both proficient weighting technique and ranking technique to achieve valid ranking result [22]. In this work a simple, yet effective, MADM method called "Simple Additive Weighting" (SAW) is applied. The SAW method is described in detail also with numerical examples in [28], and is briefly summarized in the following. According to SAW, the decision maker assigns importance weights (W_1, W_2, …,W_n) to each of the attributes. The weights are normalized so that:

$$\sum_{j=1}^{n} W_j = 1 \tag{A.1}$$

Then the decision maker makes a numerical scaling of intra-attribute values since the SAW method requires a comparable scale for all elements in the decision matrix. A simple procedure is to perform a linear scale transformation, which consists in dividing the attribute value by its maximum value:

$$R_{ij} = \frac{X_{ij}}{X_j^*} \tag{A.2}$$

where $X_j^* = \max_i X_{ij}$

This scale transformation applies only to the attributes that are defined as "benefit attributes" (e.g. the specific heat, the thermal conductivity, etc.) where the larger is the value the greater is the preference. Instead, in case of a "cost attribute" (e.g. the specific cost of the material, the dynamic viscosity, etc.) where the smaller is the value the greater is the preference, the transformed value is:

$$R_{ij} = 1 - \frac{X_{ij}}{X_j^*} \tag{A.3}$$

However, when both benefit and cost criteria exist in the decision matrix (as in our example where also the specific cost is included among the attributes) we should not use Eqs. (A.2) and (A.3) at the same time because their bases are different (0 for benefit criterion, 1 for cost). Instead, we can treat cost criteria as benefit criteria by taking the inverse of the values. Then the correct equation for cost criteria becomes:

$$R_{ij} = \frac{1/X_{ij}}{max_i\left(1/X_{ij}\right)} = \frac{min_i\left(X_{ij}\right)}{X_{ij}} = \frac{X_j^{\min}}{X_{ij}} \tag{A.4}$$

The decision maker can then obtain a total score (A_i) for each storage medium alternative simply by multiplying the scaled rating for each attribute value (R_{ij}) by the importance weight assigned to the attribute (W_{ij}), and then summing these products over all n attributes. For instance, the total score for material alternative i is:

$$A_i = \sum_{j=1}^{n} W_j \cdot R_{ij} \tag{A.5}$$

After the total scores are computed for each material alternative, the alternative with the highest score (A^*) is the most preferred alternative and is prescribed to the decision maker:

$$A^* = max_i(A_i) \tag{A.6}$$

For the best effectiveness of the SAW method it is necessary to find a reasonable basis on which to form the weights reflecting the importance of each of the attributes. Thus, the decision maker must be very careful in assigning these numerical values. SAW method is a very powerful approach to MADM when the attributes can be considered separately (i.e., when there are essentially no important complementarities).

Appendix B. Supplementary data

Supplementary data to this article can be found online at https://doi.org/10.1016/j.est.2022.104411.

References

[1] L. Miró, J. Gasia, L.F. Cabeza, Thermal energy storage (TES) for industrial waste heat (IWH) recovery: a review, Appl. Energy (2016), https://doi.org/10.1016/j.apenergy.2016.06.147.

[2] D. Wang, X. Ling, H. Peng, Performance analysis of double organic rankine cycle for discontinuous low temperature waste heat recovery, Appl. Therm. Eng. 48 (2012) 63–71, https://doi.org/10.1016/j.applthermaleng.2012.04.017.

[3] T. Sung, E. Yun, H.D. Kim, S.Y. Yoon, B.S. Choi, K. Kim, J. Kim, Y.B. Jung, K. C. Kim, Performance characteristics of a 200-kW organic rankine cycle system in a steel processing plant, Appl. Energy (2016), https://doi.org/10.1016/j.apenergy.2016.09.018.

[4] A.M. Pantaleo, J. Fordham, O.A. Oyewunmi, P. De Palma, C.N. Markides, Integrating cogeneration and intermittent waste-heat recovery in food processing: microturbines vs. ORC systems in the coffee roasting industry, Appl. Energy (2018), https://doi.org/10.1016/j.apenergy.2018.04.097.

[5] K. Couvreur, W. Beyne, M. De Paepe, S. Lecompte, Hot water storage for increased electricity production with organic rankine cycle from intermittent residual heat sources in the steel industry, Energy 200 (2020), https://doi.org/10.1016/j.energy.2020.117501.

[6] T. Keplinger, M. Haider, T. Steinparzer, A. Patrejko, P. Trunner, M. Haselgrübler, Dynamic simulation of an electric arc furnace waste heat recovery system for steam production, Appl. Therm. Eng. 135 (2018) 188–196, https://doi.org/10.1016/j.applthermaleng.2018.02.060.

[7] M. Ramirez, M. Epelde, M.G. De Arteche, A. Panizza, A. Hammerschmid, M. Baresi, N. Monti, Performance evaluation of an ORC unit integrated to a waste heat recovery system in a steel mill, Energy Procedia (2017), https://doi.org/10.1016/j.egypro.2017.09.183.

[8] T. Bause, F. Campana, L. Filippini, A. Foresti, N. Monti, T. Pelz, Cogeneration with ORC at elbe-stahlwerke feralpi EAF shop, Iron Steel Technol. 12 (2015) 290–299.

[9] T. Steinparzer, M. Haider, A. Fleischanderl, A. Hampel, G. Enickl, F. Zauner, Heat exchangers and thermal energy storage concepts for the off-gas heat of steelmaking devices, J. Phys. Conf. Ser. 395 (2012), https://doi.org/10.1088/1742-6596/395/1/012158.

[10] T. Bauer, C. Odenthal, A. Bonk, Molten salt storage for power generation, Chem. Ing. Tech. (2021), https://doi.org/10.1002/cite.202000137.

[11] W.A. Al Nahdi, M.I. Hassan Ali, Electricity and water cogeneration utilizing aluminum furnaces waste heat integrating thermal storage organic rankine cycle, J. Sustain. Dev. Energy, Water Environ. Syst. (2021), https://doi.org/10.13044/j.sdewes.d8.0381. N/A.

[12] A. Touzo, R. Olives, G. Dejean, D. Pham Minh, M. El Hafi, J.F. Hoffmann, X. Py, Experimental and numerical analysis of a packed-bed thermal energy storage system designed to recover high temperature waste heat: an industrial scale up, J. Energy Storage 32 (2020), https://doi.org/10.1016/j.est.2020.101894.

[13] I. Ortega-Fernández, J. Rodríguez-Aseguinolaza, Thermal energy storage for waste heat recovery in the steelworks: the case study of the REslag project, Appl. Energy 237 (2019) 708–719, https://doi.org/10.1016/j.apenergy.2019.01.007.

[14] A. König-Haagen, S. Höhlein, D. Brüggemann, Detailed exergetic analysis of a packed bed thermal energy storage unit in combination with an organic rankine cycle, Appl. Therm. Eng. 165 (2020), https://doi.org/10.1016/j.applthermaleng.2019.114583.

[15] G. Nardin, A. Meneghetti, F. Dal Magro, N. Benedetti, PCM-based energy recovery from electric arc furnaces, Appl. Energy (2014), https://doi.org/10.1016/j.apenergy.2014.07.052.

[16] F. Dal Magro, M. Jimenez-Arreola, A. Romagnoli, Improving energy recovery efficiency by retrofitting a PCM-based technology to an ORC system operating under thermal power fluctuations, Appl. Energy 208 (2017) 972–985, https://doi.org/10.1016/j.apenergy.2017.09.054.

[17] P. Royo, L. Acevedo, V.J. Ferreira, T. García-Armingol, A.M. López-Sabirón, G. Ferreira, High-temperature PCM-based thermal energy storage for industrial furnaces installed in energy-intensive industries, Energy 173 (2019) 1030–1040, https://doi.org/10.1016/j.energy.2019.02.118.

[18] H. Schreiber, S. Graf, F. Lanzerath, A. Bardow, Adsorption thermal energy storage for cogeneration in industrial batch processes: experiment, dynamic modeling and system analysis, Appl. Therm. Eng. 89 (2015) 485–493, https://doi.org/10.1016/j.applthermaleng.2015.06.016.

[19] M. Angerer, M. Djukow, K. Riedl, S. Gleis, H. Spliethoff, Simulation of cogeneration-combined cycle plant flexibilization by thermochemical energy storage, J. Energy Resour. Technol. 140 (2018), 020909, https://doi.org/10.1115/1.4038666.

[20] G. Hartfuß, M. Schmid, G. Scheffknecht, Off-gas waste heat recovery for electric arc furnace steelmaking using calcium hydroxide (Ca(OH)2) dehydration, Steel Res. Int. 91 (2020), https://doi.org/10.1002/srin.202000048.

[21] A.I. Fernandez, M. Martnez, M. Segarra, I. Martorell, L.F. Cabeza, Selection of materials with potential in sensible thermal energy storage, Sol. Energy Mater. Sol. Cells 94 (2010) 1723–1729, https://doi.org/10.1016/j.solmat.2010.05.035.

[22] H. Xu, A. Romagnoli, J.Y. Sze, X. Py, Application of material assessment methodology in latent heat thermal energy storage for waste heat recovery, Appl. Energy 187 (2017) 281–290, https://doi.org/10.1016/j.apenergy.2016.11.070.

[23] M.T. White, A.I. Sayma, A new method to identify the optimal temperature of latent-heat thermal-energy storage systems for power generation from waste heat, Int. J. Heat Mass Transf. 149 (2020), https://doi.org/10.1016/j.ijheatmasstransfer.2019.119111.

[24] R. Pili, A. Romagnoli, H. Spliethoff, C. Wieland, Techno-economic analysis of waste heat recovery with ORC from fluctuating industrial sources, Energy Procedia 129 (2017) 503–510, https://doi.org/10.1016/j.egypro.2017.09.170.

[25] R. Pili, A. Romagnoli, M. Jiménez-Arreola, H. Spliethoff, C. Wieland, Simulation of organic rankine cycle – quasi-steady state vs dynamic approach for optimal economic performance, Energy 167 (2019) 619–640, https://doi.org/10.1016/j.energy.2018.10.166.

[26] F. Dal Magro, S. Savino, A. Meneghetti, G. Nardin, Coupling waste heat extraction by phase change materials with superheated steam generation in the steel industry, Energy (2017), https://doi.org/10.1016/j.energy.2017.04.051.

[27] M. Angerer, M. Djukow, K. Riedl, S. Gleis, H. Spliethoff, Simulation of cogeneration-combined cycle plant flexibilization by thermochemical energy storage, J. Energy Resour. Technol. 140 (2018), https://doi.org/10.1115/1.4038666.

[28] C.L. Hwang, K. Yoon, Multiple Attribute Decision Making Methods and Applications: A State-of-the-Art Survey, 1981.

[29] F. Dinter, M. Geyer, R. Tamme, Thermal Energy Storage for Commercial Applications - A Feasibility Study on Economic Storage Systems, Springer-Verlag, Berlin, 1991.

[30] J.A. Duffie, W.A. Beckman, Solar Engineering of Thermal Processes, Fourth Edi, Wiley, 2013.

[31] H.P. Garg, S.C. Mullick, A.K. Bhargava, Solar Thermal Energy Storage, D. Reidel Publishing Company, Dordrecht, Holland, 1985.

[32] R.T. Haelsig, D.W. Halstead, R.M. Southall, G.F. von Fuchs, A.W. Warren, Developing and Upgrading of Solar System Thermal Energy Storage Simulation Models - Technical Progress Report For Period September 1, 1977 - February 28, 1978, 1978.

[33] D.E. Beasley, C. Ramanarayanan, H. Torab, Thermal response of a packed bed of spheres containing a phase-change material, Int. J. Energy Res. 13 (1989) 253–265.

[34] D.E. Jones, J.E. Hill, Testing of Pebble-bed and Phase-change Thermal Storage Devices According to Ashrae Standard 94-77, Washington, D.C. 20234, 1979.

[35] D.E. Beasley, J.A. Clark, Transient response of a packed bed for thermal energy storage, Int. J. Heat Mass Transf. 27 (1984) 1659–1669, https://doi.org/10.1016/0017-9310(84)90278-3.

[36] S.A. Mumma, W.C. Marvin, A method of simulating the performance of a pebble bed thermal energy storage and recovery system, in: American Society of

Mechanical Engineers and American Institute of Chemical Engineers, Heat Transfer Conference, ASME, St. Louis, Mo., 1976, p. 6. August 9–11.
[37] M. Geyer, A feasibility study on thermal energy storage for commercial applications, in: F. Dinter, M. Geyer, R. Tamme (Eds.), Therm. Energy Storage Commer. Appl, Springer-Verlag, Berlin, 1991, pp. 87–153.
[38] K. Allen, T. Von Backström, E. Joubert, P. Gauché, Rock bed thermal storage: concepts and costs, AIP Conf. Proc. 1734 (2016), https://doi.org/10.1063/1.4949101.
[39] M. Liu, N.H. Steven Tay, S. Bell, M. Belusko, R. Jacob, G. Will, W. Saman, F. Bruno, Review on concentrating solar power plants and new developments in high temperature thermal energy storage technologies, Renew. Sust. Energ. Rev. (2016), https://doi.org/10.1016/j.rser.2015.09.026.
[40] Oak Ridge National Laboratory, Waste Heat to Power Market Assessment, 2015.
[41] S. Ogriseck, Integration of Kalina cycle in a combined heat and power plant, a case study, Appl. Therm. Eng. (2009), https://doi.org/10.1016/j.applthermaleng.2009.02.006.
[42] D. Fiaschi, G. Manfrida, E. Rogai, L. Talluri, Exergoeconomic analysis and comparison between ORC and Kalina cycles to exploit low and medium-high temperature heat from two different geothermal sites, Energy Convers. Manag. 154 (2017) 503–516, https://doi.org/10.1016/j.enconman.2017.11.034.
[43] Eurostat, Energy statistics. https://ec.europa.eu/eurostat/data/database, 2022 (accessed February 6, 2022).